Monthly Notices
of the
ROYAL ASTRONOMICAL SOCIETY

Mon. Not. R. Astron. Soc. **402,** 985–1004 (2010) doi:10.1111/j.1365-2966.2009.15933.x

A new empirical method to infer the starburst history of the Universe from local galaxy properties

Philip F. Hopkins[1]★ and Lars Hernquist[2]

[1]*Department of Astronomy and Theoretical Astrophysics Center, University of California Berkeley, Berkeley, CA 94720, USA*
[2]*Harvard-Smithsonian Center for Astrophysics, 60 Garden Street, Cambridge, MA 02138, USA*

Accepted 2009 October 23. Received 2009 October 20; in original form 2009 September 17

ABSTRACT

The centres of ellipticals and bulges are formed dissipationally, via gas inflows over short time-scales – the 'starburst' mode of star formation. Recent work has shown that the surface brightness profiles, kinematics and stellar populations of spheroids can be used to separate the dissipational component from the dissipationless 'envelope' made up of stars formed over more extended histories in separate objects, and violently assembled in mergers. Given high-resolution, detailed observations of these 'burst relic' components of ellipticals (specifically their stellar mass surface density profiles), together with the simple assumptions that some form of the Kennicutt–Schmidt law holds and that the burst was indeed a dissipational, gas-rich event, we show that it is possible to invert the observed profiles and obtain the time- and space-dependent star formation history of each burst. We perform this exercise using a large sample of well-studied spheroids, which have also been used to calibrate estimates of the 'burst relic' populations. We show that the implied bursts scale in magnitude, mass and peak star formation rate (SFR) with galaxy mass in a simple manner, and provide fits for these correlations. The typical burst mass $M_{\rm burst}$ is $\sim$ 10 per cent of the total spheroid mass, the characteristic starburst time-scale implied is a nearly galaxy-mass-independent $t_{\rm burst} \sim 10^8$ yr, the peak SFR of the burst is $\sim M_{\rm burst}/t_{\rm burst}$ and bursts decay subsequently in power-law fashion as $\dot{M}_* \propto t^{-2.4}$. As a function of time, we obtain the spatial size of the starburst; burst sizes at peak activity scale with burst mass in a manner similar to the observed spheroid size–mass relation, but are smaller than the full galaxy size by a factor of $\sim$10; the size grows in time as the central, most dense regions are more quickly depleted by star formation as $R_{\rm burst} \propto t^{0.5}$. Combined with observational measurements of the nuclear stellar population ages of these systems – i.e. the distribution of times when these bursts occurred – it is possible to re-construct the dissipational burst contribution to the distribution of SFRs and infrared (IR) luminosity functions (LFs) and luminosity density of the Universe. We do so and show that these burst LFs agree well with the observed IR LFs at the brightest luminosities, at redshifts $z \sim 0$–2. At low luminosities, however, bursts are always unimportant; the transition luminosity between these regimes increases with redshift from the ultraluminous infrared galaxy threshold at $z \sim 0$ to hyper-luminous infrared galaxy thresholds at $z \sim 2$. At the highest redshifts $z \gtrsim 2$, we can set strict upper limits on starburst magnitudes, based on the maximum stellar mass remaining at high densities at $z = 0$, and find tension between these and estimated number counts of sub-millimetre galaxies, implying that some change in bolometric corrections, the number counts themselves or the stellar initial mass function may be necessary. At all redshifts, bursts are a small fraction of the total SFR or luminosity density, $\sim$5–10 per cent, in good agreement with estimates of the contribution of merger-induced star formation.

★E-mail: phopkins@astro.berkeley.edu

Key words: stars: formation – stars: general – galaxies: active – galaxies: evolution – galaxies: formation – cosmology: theory.

1 INTRODUCTION

Understanding the global star formation history of the Universe remains an important unresolved goal in cosmology. Of particular interest is the role played by mergers in driving star formation and/or the infrared (IR) luminosities of massive systems. A wide range of observations support the view that violent, dissipational events (e.g. gas-rich mergers) are important to galaxy evolution and, in particular, that the central, dense portions of galaxy bulges and spheroids must be formed in such events, but less clear is their contribution to the global star formation process.

In the local Universe, the population of star-forming galaxies appears to transition from 'quiescent' (undisturbed) discs – which dominate the *total* star formation rate (SFR)/IR luminosity density – at the luminous infrared galaxy (LIRG) threshold of $10^{11}\,L_{\odot}$ ($\dot{M}_{*} \sim 10$–$20\,M_{\odot}\,yr^{-1}$) to systems that are clearly merging and violently disturbed at a few times this luminosity. The most intense starbursts at $z = 0$, ultraluminous infrared galaxies (ULIRGs; $L_{IR} > 10^{12}\,L_{\odot}$), are invariably associated with mergers (e.g. Joseph & Wright 1985; Sanders & Mirabel 1996), with dense gas in their centres providing material to feed black hole growth and to boost the concentration and central phase-space density of merging spirals to match those of ellipticals (Hernquist, Spergel & Heyl 1993; Robertson et al. 2006). Various studies have shown that the mass involved in these starburst events is critical to explaining the relations between spirals, mergers and ellipticals, and has a dramatic impact on the properties of merger remnants (e.g. Lake & Dressler 1986; Doyon et al. 1994; Shier & Fischer 1998; James et al. 1999; Genzel et al. 2001; Tacconi et al. 2002; Rothberg & Joseph 2004, 2006a; Dasyra et al. 2006, 2007; Hopkins et al. 2009b, hereafter H09b; Hopkins et al. 2009e, hereafter H09e).

At high redshifts, bright systems dominate more and more of the IR luminosity function (LF; e.g. Le Floc'h et al. 2005; Pérez-González et al. 2005; Caputi et al. 2007; Magnelli et al. 2009). Merger rates increase rapidly (by a factor of $\sim$10 from $z = 0$–2; see e.g. Hopkins et al. 2009i, and references therein), leading to speculation that the merger rate evolution may in fact drive the observed evolution in the cosmic SFR density, which also rises sharply in this interval (e.g. Hopkins & Beacom 2006, and references therein). However, many LIRGs at $z \sim 1$, and possibly ULIRGs at $z \sim 2$, appear to be 'normal' galaxies, without dramatic morphological disturbances associated with the local starburst population or large apparent AGN contributions (Sajina et al. 2007; Yan et al. 2007; Dasyra et al. 2008; Dey et al. 2008; Melbourne et al. 2008). At the same time, even more luminous systems appear, including large numbers of hyper-LIRG (HyLIRG; $L_{IR} > 10^{13}\,L_{\odot}$) and bright sub-millimetre galaxies (e.g. Chapman et al. 2005; Younger et al. 2007; Casey et al. 2009). These systems exhibit many of the traits more commonly associated with merger-driven starbursts, including morphological disturbances, and may be linked to the emergence of massive, quenched (non star-forming), compact ellipticals at times as early as $z \sim 2$–4 (Papovich et al. 2005; Tacconi et al. 2006; Schinnerer et al. 2008; Younger et al. 2008; Tacconi et al. 2008; Chapman et al. 2009).

In a series of papers, Hopkins et al. (2008c, hereafter H08c), H09b and H09e, the authors combined simulation libraries of galaxy mergers with observations of nearby ellipticals to develop a methodology to empirically separate spheroids into their two dominant physical components. First, a dissipationless component, i.e. an 'envelope', formed from the violent relaxation/scattering of stars already present in merging stellar discs that contribute to the remnant. Because discs are extended, with low phase-space density (and collisionless processes cannot raise this phase-space density), these stars will necessarily dominate the profile at large radii, hence the envelope, with a low central density.

Secondly, a dissipational or 'burst' component, i.e. a dense stellar relic, formed from gas which lost its angular momentum and fell into the nucleus of the remnant, turning into stars in a compact central starburst like those in e.g. local ULIRGs (although these represent the most extreme cases). Because gas radiates, it can collapse to very high densities, and stars formed in a starburst will dominate the profile within radii of $\sim$0.5–1 kpc, accounting for the high central densities of ellipticals. The gas will reflect that brought in from merging discs, but could in principle also be augmented by additional cooling or stellar mass loss in the elliptical (see e.g. Ciotti & Ostriker 2007).

In subsequent mergers, these two stellar components will act dissipationlessly, but the segregation between the two is sufficient that they remain distinct even after multiple, major 'dry' re-mergers, i.e. one can still, in principle, distinguish the dense central stellar component that is the remnant of the combined dissipational starburst(s) from the less dense outer envelope that is the remnant from low-density disc stars.

In H08c, the methodology for empirically separating these components in observed systems is presented, and tested this on samples of nearby merger remnants from Rothberg & Joseph (2004). Comparison with other, independent constraints such as stellar population synthesis models (Titus, Spillar & Johnson 1997; Reichardt, Jimenez & Heavens 2001; Michard 2006) and galaxy abundance profiles (Foster et al. 2009; McDermid et al. 2006; Sánchez-Blázquez et al. 2007) and direct comparison of simulations with observed surface brightness profiles, galaxy shapes and kinematics are used to demonstrate that the approach can reliably extract the dissipational component of the galaxy (see Section 2.1).

If this general scenario is correct, then the empirically identified burst relic components in local spheroids represent a novel and powerful new constraint on the history and nature of dissipational starbursts. In this paper, we present and develop these constraints and, in particular, show that they are not merely integral constraints on the masses and sizes of bursts. We show that the unique nature of dissipational star formation, together with the existence of some Kennicutt–Schmidt-type relation between gas surface densities and SFRs, means that the relic profiles can be *inverted* to obtain the full time and radius-dependent star formation history of each galaxy starburst (Section 2). We present the resulting, derived burst star formation histories for samples of hundreds of local, well-observed galaxy spheroids. We show that such starbursts follow broadly similar time-dependent behaviour, with characteristic starburst SFRs, durations, rise and decay rates, and spatial sizes that scale with galaxy mass and other properties according to simple scaling laws across approximately five decades in starburst and spheroid mass (Section 3.2). Combining these inferred star formation histories

(and resulting burst light curves) with empirical determinations of the ages of each starburst, we can reconstruct the starburst history of the Universe, including e.g. the LFs of such dissipational bursts at all redshifts and their contribution to the global SFR density (Section 3.3). We discuss the uncertainties in this approach, compare with the previous, independent attempts to constrain these quantities via other observational methods and summarize our results in Section 4.

Throughout, we adopt a $\Omega_{\rm M} = 0.3, \Omega_{\Lambda} = 0.7, h = 0.7$ cosmology and a Chabrier (2003) stellar initial mass function (IMF), but these choices do not affect our conclusions.

2 THE OBSERVATIONS AND METHODOLOGY

2.1 The observations

As discussed in Section 1, spheroid mass profiles can be decomposed into a central relic starburst and an outer stellar envelope. The two components are distinct physically in the sense that the amount and distribution of the two are determined by dissipational and dissipationless dynamics, respectively. In H08c, H09b and H09e, the authors compile large samples of ellipticals from the studies of Kormendy et al. (2009) and Lauer et al. (2007) and present decompositions for these galaxies. We adopt these results for the present study.

Briefly, Kormendy et al. (2009) present a *V*-band Virgo elliptical survey, based on the complete sample of Virgo galaxies down to extremely faint systems in Binggeli, Sandage & Tammann (1985) (the same sample studied in Côté et al. 2006; Ferrarese et al. 2006). Kormendy et al. (2009) combine observations from a large number of sources (including Davis et al. 1985; Lauer 1985; Bender, Doebereiner & Moellenhoff 1988; Caon, Capaccioli & Rampazzo 1990; Peletier et al. 1990; Caon, Capaccioli & D'Onofrio 1994; Lauer et al. 1995, 2005; Kormendy et al. 2005; Liu et al. 2005) and new photometry from the McDonald Observatory, the *Hubble Space Telescope* (*HST*) archive and the Sloan Digital Sky Survey (SDSS) for each of their objects which, after careful conversion to a single photometric standard, enables accurate surface brightness measurements over a wide dynamic range (with an estimated zero-point accuracy of ± 0.04 *V* mag arcsec^{-2}). Typically, the galaxies in this sample have profiles spanning $\sim$12–15 mag in surface brightness, corresponding to a range of nearly four orders of magnitude in physical radii from $\sim$10 to $\sim$100 kpc, permitting the best simultaneous constraints on the shapes of both the outer and inner profiles of any of the objects we study. Unfortunately, since this is restricted to Virgo ellipticals, the number of galaxies is limited, especially at the intermediate and high end of the mass function.

We therefore include surface brightness profiles from Lauer et al. (2007), further supplemented by Bender et al. (1988). Lauer et al. (2007) compile *V*-band measurements of a large number of nearby systems for which *HST* imaging of galactic nuclei is available. These include the Lauer et al. (2005) Wide Field Planetary Camera 2 (WFPC2) data set, the Laine et al. (2003a) WFPC2 brightest cluster galaxy sample (in which the objects are specifically selected as brightest cluster galaxies from Postman & Lauer 1995), and the Lauer et al. (1995) and Faber et al. (1997) WFPC1 compilations. Details of the treatment of the profiles and conversion to a single standard are given in Lauer et al. (2007). *HST* images are combined with ground-based measurements (see the above references) to construct profiles that typically span physical radii from $\sim$10 to $\sim$10–20 kpc. The sample includes ellipticals over a wide range of luminosities, down to $M_B \sim -15$, but is dominated by intermediate and giant ellipticals and S0 galaxies, with typical magnitudes $M_B \lesssim -18$.

H08c, H09b and H09e apply various tests to demonstrate that the profile decompositions are robust. Systematic comparison with large suites of hydrodynamic simulations as calibrators implies that the derived burst masses and radial profiles are accurate to within a factor of $\sim$2. Independent, purely empirical analyses of these profiles (Kormendy et al. 2009) and those of similar objects (e.g. Ferrarese et al. 2006; Balcells, Graham & Peletier 2007a) yield similar conclusions. For most of the objects in our data set, the profiles include e.g. ellipticity, a_4/a and $g - z$ colours as a function of radius, as well as kinematic information. In Kormendy et al. (2009), H09b and H09e, the authors show that these secondary properties exhibit transitions that mirror the fitted decompositions (e.g. transitions to discier, more rotationally supported, younger inner components).

Likewise, comparison with detailed resolved stellar population properties – i.e. independent constraints from stellar population synthesis models, abundance gradients and galaxy colours – yields good agreement where available (Schweizer 1996; Titus et al. 1997; Schweizer & Seitzer 1998; Reichardt et al. 2001; McDermid et al. 2006; Michard 2006; Reda et al. 2007; Sánchez-Blázquez et al. 2007; Schweizer & Seitzer 2007; Foster et al. 2009). Moreover, in young merger remnants, where stellar populations and colours more clearly indicate the post-starburst component, the methodology works well (Rothberg & Joseph 2004; Rothberg & Joseph 2006a,b; H08c). In H09b and H09e, these results are also checked against profile data used in Bender et al. (1988), Bender, Burstein & Faber (1992, 1993) and Bender, Saglia & Gerhard (1994). The latter are more limited in dynamic range, but allow for construction of multi-colour profiles in e.g. *V*, *R* and *I* bands, to test whether they are sensitive to the band used and to construct e.g. stellar mass and M_*/L profiles.

We illustrate our methodology in Fig. 1. First, we show a typical stellar mass surface density profile of an $\sim L_*$ elliptical galaxy, from the sample of Lauer et al. (2007). We plot the decomposition into burst and extended envelope (violently relaxed) components, together with some of their integral properties (stellar mass fractions, effective radii and fitted profile shapes in the form of the best-fitting Sersic index). We compare the observed system to the stellar mass density profile of one of the hydrodynamic simulations presented in H09b. The simulation is determined in that paper to be similar in total mass, profile shape and kinematic properties to the observed system (see table 1 therein). In the simulation, the true, physical starburst component from gas that loses angular momentum and falls to the centre at coalescence is known, as is the non-starburst component from violently relaxed stars present in the discs before the final merger. We show the separate contributions of the two components to the stellar mass density. The agreement is good, lending confidence to our empirical decomposition procedure and allowing us to consider the simulations as a reasonable calibration sample for our approach.

2.2 Basic assumptions

Taking the observationally estimated burst component, this defines a relic surface density $\Sigma_{\rm burst}(R)$. Of course, in general, the star formation history that yields a given stellar surface density is non-unique. But if we make three simple, physically and observationally motivated assumptions, $\Sigma_{\rm burst}(R)$ can be inverted into a space- and time-dependent burst star formation history.

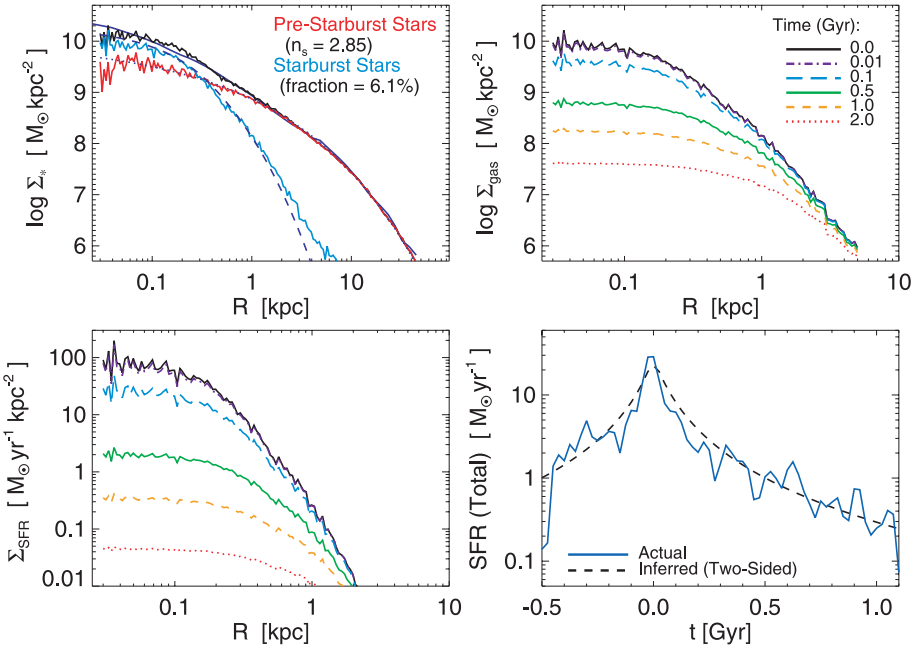

Figure 1. Illustration of the methodology used in this paper. Top left: observed stellar mass profile of a typical $\sim L_*$ elliptical from the Lauer et al. (2007) sample (dark blue solid). We show the empirical, fitted decomposition into inner 'starburst relic' (dark blue dashed) and outer violently relaxed (dark blue dotted) components, from H09b,e. We compare a simulation which yields a remnant with similar profile, kinematics and stellar populations (total mass profile in black). For the simulation, we know the true, dissipational merger-induced starburst component (light blue, with labelled mass fraction) and dissipationless violently relaxed component from stars formed before the final merger (red, with the labelled Sersic index). The fitting and simulation-matching procedures yield similar burst decompositions. Top right: implied gas surface density profile of the burst (*ignoring* the violently relaxed component, formed over much more extended periods) as a function of time. At time $t = 0$ (defined as the time where the implied SFR peaks), we assume that the burst relic was in place mostly as gas. Given the observed Kennicutt (1998) relation, this yields an SFR surface density at each location. The gas density then declines as gas is turned to stars. Integrating forwards, we obtain the gas (and formed stellar) mass distribution at each later time (labelled). Bottom left: corresponding SFR surface density profile. We also label the half-SFR radius at each time. Bottom right: implied *total* SFR (integrating the SFR density profile over radius), at each time (black dashed). The 'two-sided' estimate assumes a light curve with a symmetric rise/fall. We compare the true simulation SFR versus time in the best-fitting simulation. The two agree well – despite the simple nature of the model, it appears to be reliable in simulations with more detailed physics, and allows us to recover the star formation history of a given spheroid starburst from its relic mass profile.

These assumptions are as follows.

(1) Some form of the Kennicutt (1998) law holds for these objects, relating their SFR surface density $\dot{\Sigma}_*$ to their gas surface density $\Sigma_{\rm gas}$.

(2) The relic burst mass is dominated by an order of one most massive event, i.e. is not constituted from the later assembly of many independent, well-separated bursts nor by an extended series of independent, well-separated bursts in the same galaxy. There may be many small events, but most of the mass should come from a single, dominant event.

(3) This event, at its inception, involved the central regions being (however briefly) gas-dominated. In other words, the burst began from a gas-dominated central density and formed largely *in situ*, rather than from an extended, low-gas-density trickle in which the gas density was never nearly as large as the total/final stellar mass density.

In detail, these assumptions are not exactly correct (we discuss this further in Section 4), but most observational constraints indicate that deviations from them are at the factor of approximately a couple level, comparable to or less than e.g. most of the systematic uncertainties in the observations to which we will compare.

Regarding assumption (1), observations indicate that at both low (e.g. Kennicutt 1998; Bigiel et al. 2008; Bothwell, Kennicutt & Lee 2009, and references therein) and high ($z \sim 2$–4; e.g. Bouché et al. 2007) redshifts, a Kennicutt–Schmidt star formation law applies over a large dynamic range in stellar mass and SFRs (from $\sim$1 to $3000\,{\rm M}_\odot\,{\rm yr}^{-1}$). These observations have also shown that the same relation pertains to a diverse array of objects, from dwarf galaxies, through local gas-poor discs; to near 'quenched' red systems; to clumpy, turbulent high-redshift discs and irregular systems; to merger-induced starbursts and ULIRGs; and to high-redshift submillimetre galaxies, among others. The extent of the uncertainty appears to be in the precise normalization/slope of the relation (with the above references favouring power-law slopes varying from $\sim$1.4 to 1. 7). We take this uncertainty into account below and show that it has a relatively minor effect on our conclusions. The Kennicutt (1998) relation may break down at very low surface densities, where there is some star formation threshold, but our analysis here is specifically for very high surface density systems.

Regarding assumption (2), this is well motivated by a combination of theoretical models and observations of galaxy stellar populations and structural properties. In most models, nuclear burst masses are dominated by the largest, most recent event (see e.g. Khochfar & Burkert 2003; Croton et al. 2006; de Lucia & Blaizot 2007; Somerville et al. 2008; Hopkins et al. 2009i). Mergers and other violent processes that can drive large quantities of gas into galaxy centres are not so common as to yield many bursts of equal strength, and even if systems had earlier bursts at much higher redshifts, they would have grown by a large factor in mass since those times, such that the most recent event would dominate (see the above references and Weinzirl et al. 2009; Hopkins et al. 2009i).

Observationally, evidence from nuclear kinematics and profile shapes supports the view that most of the mass in spheroid starburst components, especially in the cusp ellipticals that dominate (>90 per cent) the total mass density of spheroids and bulges, was assembled *in situ* by the most recent starburst, without significant modification since that time (e.g. Faber et al. 1997; Simien & Prugniel 1997a,b,c; Kormendy 1999; Quillen, Bower & Stritzinger 2000; Ravindranath et al. 2001; Rest et al. 2001; Laine et al. 2003a; Emsellem et al. 2004, 2007; Lauer et al. 2005; Ferrarese et al. 2006; McDermid et al. 2006; Cappellari et al. 2007; Côté et al. 2007; Lauer et al. 2007; Hopkins, Cox & Hernquist 2008a; Kormendy et al. 2009). Even in core ellipticals, thought to have been affected by subsequent re-mergers, the kinematics require relatively little mixing of major populations, of the order of a couple of similar mass merged systems (i.e. introducing a factor of ∼2 uncertainty) – more minor mergers may be dynamically important, but will (by definition) contribute little mass.

Most important, this assumption is supported by direct observations which indicate that the central component is well matched by a single stellar population (with the background galaxy – i.e. the violently relaxed component – being some older population), usually better so than by modelling it as having resulted from star formation extended in time (Trager et al. 2000; Nelan et al. 2005; Gallazzi et al. 2005, 2006; Lauer et al. 2005; Thomas et al. 2005; Kuntschner et al. 2006; McDermid et al. 2006). The metallicities and α-enhancements of these regions require that the stars there formed rapidly, in short-lived events or in events closely spaced in time (later series of bursts or independent well-spaced events, being ruled out by the enrichment patterns).

Regarding assumption (3), the observations argue that the system must have been (at least briefly) dominated by a strong gas inflow that then formed stars more or less *in situ*. The short time-scales of star formation indicated by stellar populations do not allow for a trickle of gas over an extended period of time. If assumption (1) applies, the corresponding star formation time-scale required to match the abundances is close to that obtained if all the gas were in place at once, and formed stars according to the Kennicutt (1998) relation – i.e. the shortest allowable time-scale. Moreover, in hydrodynamic simulations of galaxy–galaxy mergers or dissipational collapse, this is almost always the case – gas flows in on the local free-fall time. However, star formation is inefficient on the free-fall time-scale (the Kennicutt 1998 relation implying star formation efficiencies of ∼3–10 per cent per free-fall time), and so catches up over a short period following the initial gas-rich phase of inflow. In addition, the discy, rotational kinematics distinctive of the burst relics require *in situ* formation from initially gas-rich configurations (see e.g. Cox et al. 2006; Naab, Jesseit & Burkert 2006; H09e).

Note that the assumptions outlined here clearly do not apply for stars not formed in bursts. Although observations suggest that the Kennicutt (1998) law applies (although there may be a surface density threshold for star formation), it is established, in contrast to the central, burst populations, that the extended, violently relaxed stars *were* formed through star formation histories more extended in time. Discs, of course, are fed through continuous accretion, rather than a single massive inflow, so both assumptions (2) and (3) break down. Moreover, the outer components of ellipticals are formed via violent relaxation – i.e. by definition from merging already-formed stars from other galaxies – and so have no reason to be a homogeneous population. In fact, especially in massive ellipticals, it is cosmologically expected that such portions of the galaxy are made up of debris from many small systems (Gallagher & Ostriker 1972; Hernquist et al. 1993; De Lucia et al. 2006; Khochfar & Silk 2006; de Lucia & Blaizot 2007; 2009f,h; Naab, Johansson & Ostriker 2009). It is then likely that these components – ∼90 per cent of the stars, in typical $\sim L_*$ systems – have star formation histories that are not trivially invertible.

2.3 Methodology

Together, these assumptions allow us to invert an observed $\Sigma_{\rm burst}(R)$. If the relic burst mass is dominated by of order a single major event, and that event was indeed a dissipational, gas-rich and/or rapid event, then the gas density at the beginning of the burst (which we define for now, arbitrarily, as $t = 0$) should be given approximately by

$$\Sigma_{\rm gas}(R,\, t=0) \approx \Sigma_{\rm burst}(R). \quad (1)$$

The Kennicutt (1998) law relates the SFR surface density – and hence the gas depletion rate – to the gas surface density through

$$\dot{\Sigma}_* = -\frac{\rm d}{{\rm d}t}\Sigma_{\rm gas} \approx 1.5\times10^{-4}\,{\rm M_\odot\,yr^{-1}\,kpc^{-2}}\left(\frac{\Sigma_{\rm gas}}{\rm M_\odot\,pc^{-2}}\right)^{n_{\rm K}}, \quad (2)$$

where the normalization comes from Kennicutt (1998) corrected for our adopted Chabrier (2003) IMF, here chosen fixed for Milky-Way-like systems (where the relation is best calibrated). The index $n_{\rm K} \approx 1.4$ is suggested by observations of the local and intermediate-redshift Universe, and so we will adopt this as our fiducial value. However, a higher index of $n_{\rm K} \approx 1.7$ has been suggested from observations (albeit more uncertain) of systems at high redshifts with extremely intense SFRs (Bouché et al. 2007); we therefore compare our results to those obtained for such a higher $n_{\rm K}$.

Note that since we are ultimately interested in the relic SFR and time-averaged gas depletion rate, stellar mass loss can be absorbed into the normalization of the SFR–surface density relation (in essence, adopting the instantaneous recycling approximation). But, in general, we find that for reasonable recycling fractions from e.g. the models of Bruzual & Charlot (2003), the resulting differences are less than those between the choice of the slope $n_{\rm K}$. Likewise, the effects of long-term stellar mass loss (although, post-burst, a typical IMF will yield just ∼20 per cent stellar mass loss) are generally smaller than uncertainties arising from our primary assumptions above. Fortunately, the uncertainties in both (e.g. the singularity of the burst versus degree of stellar mass loss) have opposing signs, so experimenting with reasonable variations in each yields little net difference in our predictions.

With this relation, we can then integrate forwards in time from the initial gas density in each annulus, computing new gas and stellar densities after some time interval and then determining a new $\dot{\Sigma}_*$ in that annulus. We show the results of this procedure for our illustrative example in Fig. 1. At the initial time, the gas density is given by the surface density profile of the relic starburst component isolated from the observed profile (as seen in the figure, it makes no difference if we take the empirical fit or starburst component derived from the best-fitting simulation). As discussed above, we subtract out the non-starburst component. This leads to a corresponding SFR surface density. This depletes gas, leading to a lower gas surface density. The evolution is most rapid in the central regions, where the densities are highest, because the Kennicutt–Schmidt relation is super-linear in surface density. At several times, we plot the remaining gas and corresponding SFR surface densities, which both decrease and become more extended as the dense, central regions become depleted.

Integrating the SFR surface density over R at each time, we obtain the total SFR in the burst at $t \geq 0$:

$$\dot{M}_* = \int_0^\infty \dot{\Sigma}_* \, 2\pi \, R \, \mathrm{d}R. \quad (3)$$

Moreover, if we assume that light, in the UV, radio or IR, traces the SFR locally in some annulus, using e.g. the relation

$$L_{\rm IR} \approx 1.14 \times 10^{10} \, \mathrm{L}_\odot \left(\frac{\dot{M}_*}{\mathrm{M}_\odot \, \mathrm{yr}^{-1}} \right) \quad (4)$$

from Kennicutt (1998) [adjusted as appropriate for the Chabrier (2003) IMF adopted here], we then we obtain the light distribution and can evaluate e.g. the half-luminosity radius at each instant in time.[1]

Fig. 1 shows the resulting total SFR as a function of time. Note that the above procedure, strictly speaking, defines only a one-sided SFR for $t > 0$ – i.e. times later than some initial burst peak, $\dot{M}_*(t > 0)$. Real starbursts, of course, have a rise as well as a fall after their peaks, and simulations (as well as simple dynamical considerations) indicate that – to lowest order – the rises and falls are roughly symmetric (di Matteo et al. 2007; Cox et al. 2008). If we assume such symmetry, it is trivial to convert our solution for the burst from $t > 0$ to that for all times, as follows.

Our modelling gives a one-sided solution for the SFR versus time at $t > 0$, namely $\dot{M}_*|_{\rm onesided}(t > 0) \equiv f(t > 0)$. Physically, our symmetry assumption means that half the time at each luminosity is spent on each side of the peak. Quantitatively, for $t < 0$ (pre-peak), the SFR $\dot{M}_*(t \,|\, t < 0) \rightarrow f(-t/2)$, and for $t > 0$ (post-peak), $\dot{M}_*(t \,|\, t > 0) \rightarrow f(+t/2)$. This is the symmetric or 'two-sided' light curve. This choice guarantees that the *total* stellar mass formed in the burst is preserved and enforces the symmetry constraint. It is, therefore, appropriate for comparison to full time-dependent light curves. However, we stress that for *all* the quantities derived in what follows, it makes no difference whether we assume a one-sided or symmetric two-sided light curve. The duration of the burst is the same. (If it is defined as some $t_{\rm burst}$, we simply have to change our notation from referring to $t = 0$ to $t = t_{\rm burst}$, to $t = -t_{\rm burst}/2$ to $t = +\,t_{\rm burst}/2$, but the zero-point of time is arbitrary in any case.) Moreover, for the purposes of LFs and SFR densities, the relevant quantity is the time spent in each SFR interval – this is, by definition, identical whether or not we split that time across two sides of a peak.

We compare the integrated SFR as a function of time from our illustrative example in Fig. 1, inferred from the relic starburst profile, to the true simulation SFR as a function of time in the full hydrodynamic simulation that produces such a profile. The agreement is excellent, verifying our procedure. This is despite the fact that, in the full simulation, many of our assumptions are not true in detail. For example, the simulations obey a local (not global) Kennicutt–Schmidt law; thus clumping and instabilities can accelerate star formation locally. The simulations also account for feedback from stars, stellar winds and black hole accretion, which can remove and recycle gas. The SFR is not precisely trivial or monotonic in time. And the gas inflows do not occur instantaneously (so that the burst would start exactly from pure gas at $t = 0$, as assumed here). Nevertheless, it is clear that these details lead to almost no deviation between the true SFR versus time and that inferred from our simple procedure, given the observed relic starburst/inner component of the system. This is in part because some of these effects are small. Also, several tend to offset one another, so that, *on average*, the dominant physical considerations are the validity of an average Kennicutt–Schmidt law and the rapid, initially gas-rich nature of dissipational starbursts.

[1] More sophisticated, luminosity and galaxy property-dependent conversions have been proposed, but they largely differ at low IR luminosities in e.g. extended discs. Since the systems of interest here are massive starbursts, we find that the alternative conversions from e.g. Buat & Burgarella (1998) or Jonsson et al. (2006) make no difference to our conclusions.

3 RESULTS

3.1 Typical behaviour: some examples

Fig. 2 illustrates the results of our starburst inversion procedure for a representative sub-sample of the Kormendy et al. (2009) Virgo

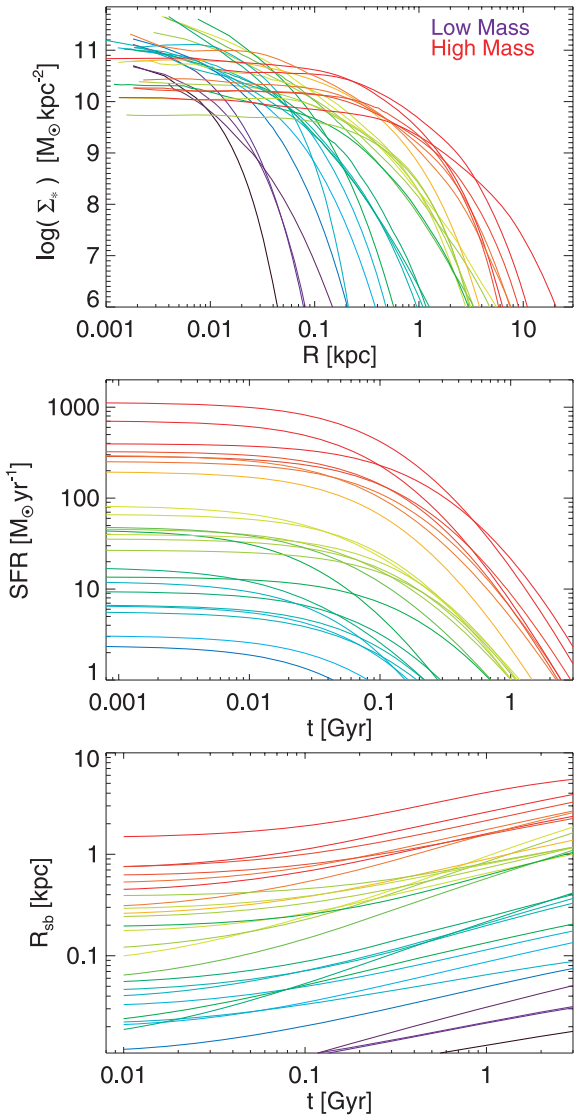

Figure 2. Typical results from recovering the burst star formation histories of spheroids. Top: surface stellar mass density profiles of the empirically fitted burst component alone, for each observed galaxy in the Kormendy et al. (2009) Virgo elliptical sample. Colours denote the total mass of each spheroid, from 10^9 $\mathrm{M}_\odot$ (violet) to $\sim 10^{12}$ $\mathrm{M}_\odot$ (red). Middle: implied burst SFR versus time since the peak of the starburst. The behaviour is roughly self-similar and well approximated by equation (5). Bottom: burst size scale (radius enclosing half the total star formation) versus time. A similar scaling applies (equation 8).

ellipticals. We first show (top) the stellar mass surface density profiles of the inner/dissipational/burst component in each object (*not* the total stellar mass density profile), as obtained using the two-component decomposition in H09b and H09e, over the dynamic range covered by the observations from Kormendy et al. (2009). In other words, we have already subtracted off the empirically estimated non-burst stellar component. For each system, using the methodology described in Section 2, we convert the inferred surface brightness profile to a time-dependent total SFR, as illustrated in Fig. 1. We show the one-sided ($t > 0$) SFR versus time so obtained, in a logarithmic scale (this highlights the relevant power-law behaviour). The total burst SFRs decay from some initial maximum in a power-law-like fashion. We find that good fits can be obtained to the time-dependent light curves with the functional form

$$\dot{M}_*(t) = \frac{\dot{M}_*(0)}{[1+(t/t_0)]^{\beta}} \Longleftrightarrow \frac{\dot{M}_*(0)}{[1+(|t|/[t_0/2])]^{\beta}}. \quad (5)$$

The first is a one-sided light curve appropriate if the burst occurs only for $t > 0$ and the second is a two-sided curve symmetric about $t = 0$ (see Section 2). The two functional forms shown are statistically equivalent for our purposes, and we therefore refer to them interchangeably. Fitting such a curve to each profile in Fig. 2, the best-fitting curves are indistinguishable on the scale shown from the numerical calculations. We discuss the best-fitting values below, but in general note that the systems tend to cluster around a power-law decay with $\beta \sim 2.5$ and clearly exhibit a characteristic decay time-scale of $\sim$0.1 Gyr.

Note that, with such a functional form, there are straightforward relations among several parameters. The half-life of the starburst $t_{1/2}$, i.e. the time for the starburst to decay to half of its maximum luminosity/SFR, is simply

$$t_{1/2} = \left(2^{1/\beta} - 1\right)\, t_0. \quad (6)$$

Likewise, the peak SFR of the burst, $\dot{M}_*(0)$, can be trivially related (knowing the burst duration $t_{1/2}$ and β) to the total stellar mass formed in the burst, via the integral constraint that $M_{\rm burst} = \int_0^{\infty} \dot{M}_*(t)\,{\rm d}t$, giving

$$\dot{M}_*(0) = (\beta - 1)\,\frac{M_{\rm burst}}{t_0} = \left[(\beta-1)\,\left(2^{1/\beta}-1\right)\right]\,\frac{M_{\rm burst}}{t_{1/2}}. \quad (7)$$

For convenience, we will use $t_{1/2}$ as our time-scale of interest below, as it has a straightforward interpretation independent of β. Moreover, for the β values of interest, the coefficient $[(\beta-1)(2^{1/\beta}-1)]$ in equation (7) is nearly constant at $\approx$0.45–0.50.

At each time, we can also estimate the effective radius of the starburst region; we specifically define this as the half-luminosity radius, where we assume that the surface luminosity density (in e.g. the IR) is proportional to the gas surface density at each instant. We show this as well (bottom) in Fig. 2. In analogy to the total fitted SFR, we can similarly describe this evolution by a power law of the form

$$\dot{R}_{\rm sb}(t) = R_{\rm sb}(0)\left[1+(t/t_{0,\,r})\right]^{\beta_{\rm r}}. \quad (8)$$

The radius doubling time $t_{1/2,\,r}$ is trivially related to $t_{0,\,r}$ by the same relation as equation (6), i.e. $t_{1/2,\,r} = (2^{1/\beta_{\rm r}} - 1)\,t_{0,\,r}$.

3.2 Properties of bursts versus mass and scale

3.2.1 Masses, time-scales and star formation rates

Fig. 3 illustrates these fits and a number of global properties of the bursts, using our full sample of profiles taken from Kormendy et al. (2009) and Lauer et al. (2007). We also present the relevant fits and scaling relations in Table 1. First, Fig. 3 shows the *total* burst mass (i.e. total mass of the inner/dissipational component)

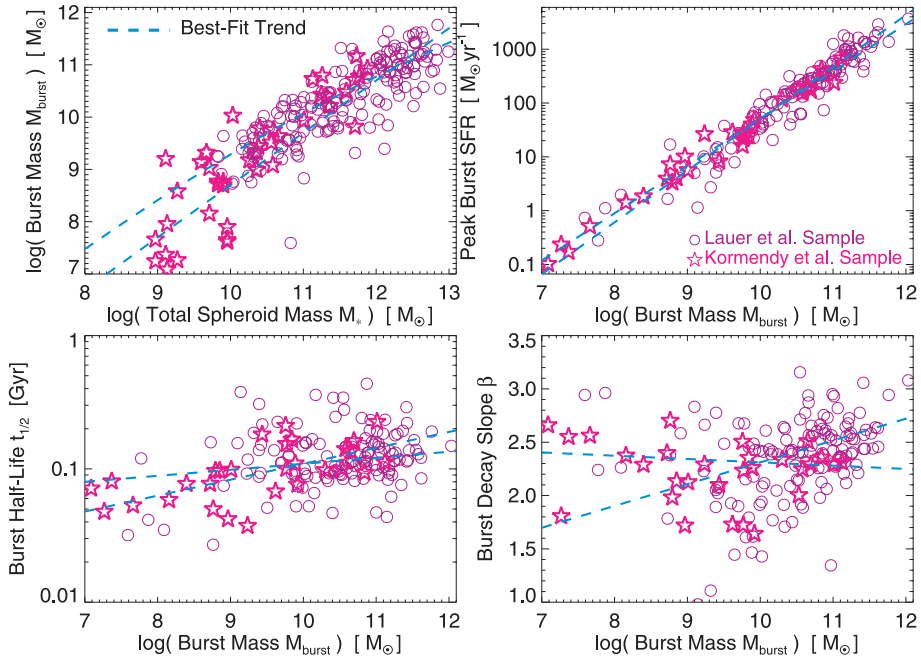

Figure 3. Observationally inferred properties of spheroid starbursts as a function of mass, from the relic starbursts. Top left: mass of the starburst component of spheroids as a function of the total spheroid stellar mass. Detailed determinations and tests of these component decompositions are presented in H09b and H09e. We show results for the Virgo galaxy sample of Kormendy et al. (2009, red stars) and local massive spheroid sample of Lauer et al. (2007, violet circles). Dashed blue lines show the range of best-fitting scalings to the observed systems (given in Table 1). Top right: peak SFR of the starburst, as a function of the total starburst mass. Bottom left: duration of the starburst (time from peak to half-peak SFR). Bottom right: best-fitting power-law slope to the decay of the SFR versus time (equation 5).

Table 1. Starburst scaling relations.

y	x	a	b	σ
$\log(M_{\rm burst}/10^{10}\,{\rm M}_\odot)$	$\log(M_*/10^{11}\,{\rm M}_\odot)$	-0.05 ± 0.12	0.78 ± 0.16	0.41
$\log(\dot{M}_*[0]/{\rm M}_\odot\,{\rm yr}^{-1})$	$\log(M_{\rm burst}/10^{10}\,{\rm M}_\odot)$	1.70 ± 0.05	0.92 ± 0.04	0.22
$\log(t_{1/2}/{\rm Gyr})$	$\log(M_{\rm burst}/10^{10}\,{\rm M}_\odot)$	-0.96 ± 0.04	0.08 ± 0.04	0.20
$\log(\dot{M}_*[0])$	$\log(M_{\rm burst}/t_{1/2})$	-0.24 ± 0.01	1.00 ± 0.01	0.04
β	$\log(M_{\rm burst}/10^{10}\,{\rm M}_\odot)$	2.38 ± 0.12	0.09 ± 0.11	0.35
$\log(R_{\rm relic}/{\rm kpc})$	$\log(M_{\rm burst}/10^{10}\,{\rm M}_\odot)$	-0.43 ± 0.07	0.58 ± 0.07	0.29
$\log(R_{1/2}/{\rm kpc})$	$\log(M_{\rm burst}/10^{10}\,{\rm M}_\odot)$	-0.57 ± 0.07	0.60 ± 0.06	0.26
$\log(t_{1/2,\,r}/{\rm Gyr})$	$\log(M_{\rm burst}/10^{10}\,{\rm M}_\odot)$	-1.07 ± 0.08	0.10 ± 0.08	0.28
$\beta_{\rm r}$	$\log(M_{\rm burst}/10^{10}\,{\rm M}_\odot)$	0.45 ± 0.01	-0.035 ± 0.017	0.11
$\log$(Burst age/Gyr)	$\log(M_*/10^{11}\,{\rm M}_\odot)$	0.95 ± 0.11	0.15 ± 0.04	0.12
Burst age/Gyr	$\log(M_*/10^{11}\,{\rm M}_\odot)$	9.5 ± 0.4	3.0 ± 0.6	2.1

Note. For the parameters x and y, the best-fitting linear scaling of $y(x)$ is presented, with the assumed functional form $y = a + b\,x$. Errors on the fitted parameters a (normalization) and b (slope) are given, along with the intrinsic scatter in y about this correlation, σ.

as a function of the total galaxy stellar mass (top left). These values, and independent tests of their validity, as well as comparison to models of spheroid formation and observed disc gas fractions, are discussed extensively in Hopkins et al. (2008a), H08c, H09b, Hopkins et al. (2009d) and H09e. To lowest order, a fraction of $\sim$10 per cent is typically in the burst/dissipational component, i.e. $M_{\rm burst} \sim 0.1\,M_*$. For somewhat higher accuracy, we use the fit from Hopkins et al. (2008a), motivated by comparison with disc gas fractions that constitute burst progenitors,

$$M_{\rm burst} \approx \frac{1}{[1+(M_*/10^{9.15}\,{\rm M}_\odot)^{0.4}]}. \quad (9)$$

This is also shown in Fig. 3, along with the simpler linear fit.

Next, we show the burst half-life $t_{1/2}$ (bottom left), as a function of burst mass (the comparison versus total stellar mass is similar, but other possible correlations are less significant). To lowest order this is mass-independent, with a value of $\sim10^8$ yr – depending on the definition, this equates to a total observable burst lifetime of a couple of 10^8 yr with an inherent factor of $\sim$2–3 scatter. Fitting to a power law, we find some (weak) mass dependence

$$t_{1/2} \approx 1.1\times10^8\,{\rm yr}\left(\frac{M_{\rm burst}}{10^{10}\,{\rm M}_\odot}\right)^{0.1}, \quad (10)$$

with a mass-independent scatter of $\sigma_{t_{1/2}} \approx 0.2$ dex about this median relation.

This agrees well with expectations from e.g. numerical simulations and extrapolation of the Kennicutt (1998) law that the burst duration should reflect the dynamical times in the central regions of galaxies; for example, a disc galaxy dynamical time $\propto R_{\rm e}/V_c$ is only weakly mass-dependent ($\propto M_*^{(0.05-0.08)}$, if we compare $R_{\rm e}\propto M_*^{0.31}$ and $V_c\propto M_*^{0.25}$ from Courteau et al. 2007; see also Bell & de Jong 2001; McGaugh 2005; Avila-Reese et al. 2008). Moreover, the scatter in the dynamical times expected from these correlations is similar to that in Fig. 3.

We next show the slope of the power-law decay, β (bottom right). There is no obvious correlation with burst mass or any other parameter; however, the values cluster in a reasonably narrow range, $\beta\sim$ 2–3, with a best-fitting median of $\beta\approx2.38$. Again, this matches expectations; given some Schmidt-law star formation relation, the slope β follows from the profile shape of the relic burst component. These profile shapes, and their physical origins, are discussed extensively in H08c and H09b; there, the authors show that they can be reasonably well parametrized as Sersic functions with relatively low Sersic indices $n_{\rm s}\sim$ 1–3 and that this follows naturally from the fact that they form via gas inflow and dissipation. Given such a Sersic-index profile, although there are no trivial analytic solutions for β, a simple numerical calculation shows that $\beta\approx$ 2–3 is the natural, corresponding expectation.

We next consider the peak burst SFR, $\dot{M}_*(0)$ (top right). Immediately, it is clear that this is very tightly correlated with the total burst mass $M_{\rm burst}$. We compare the correlation expected from equation (7), assuming a typical $\beta\approx2.4$ such that $(\beta-1)(2^{1/\beta}-1)\approx0.5$, i.e. $\dot{M}_*(0)\approx0.5\,M_{\rm burst}/t_{1/2}$. We show this both for an assumed constant $t_{1/2}=5\times10^7$ yr and for $t_{1/2}$ given by the weakly mass-dependent fit in equation (10). Both cases agree very well with the observed trend, with a small, mass-independent scatter of $\sigma_{\dot{M}_*(0)}\approx$ 0.15–0.2 dex.

Worth noting is that, within massive observed systems, peak burst SFRs of $>1000\,{\rm M}_\odot\,{\rm yr}^{-1}$ are obtained, but there is a large dynamic range – low-mass systems can have 'bursts' with implied peak SFRs as low as $\sim$0.1–1 ${\rm M}_\odot\,{\rm yr}^{-1}$. Also, since there is relatively little variation in $t_{1/2}$ at fixed mass, the scatter is, as mentioned above, small. Producing a very high SFR burst therefore requires an extremely high-gas-mass system; the case where a lower mass system might compress its gas much more efficiently, leading to a shorter lived but arbitrarily highly peaked burst, appears to be rare.

Finally, we note that their is some (factor of $\sim$2) observational uncertainty in the exact normalization of the correlation between the SFR and gas surface densities. Adopting a different IMF will likewise systematically shift the inferred relation from Kennicutt (1998). However, so long as the change in equation (2) is purely in normalization, it has no effect on the shape of the inferred light curves, and translates directly to corresponding normalization changes in the resulting SFR and time-scales in Figs 2–4 and Table 1. Specifically, if the normalization in equation (2) is multiplied by a factor η, then the implied peak SFR $\dot{M}_*[0]$ increases by the same factor η and the burst time-scale $t_{1/2}$ (and $t_{1/2,\,r}$) decreases by a factor η. All other parameters in Table 1 are unchanged.

3.2.2 *Spatial sizes of bursts*

Fig. 4 continues our analysis, plotting parameters as in Fig. 3 but for the burst spatial sizes. First, we consider the effective (projected half-stellar mass) radius of the burst remnant (top left), i.e. the radius of *all* stars after the burst has completed, namely of the relic profile as shown in Fig. 2 (top left). We consider this as a function of burst

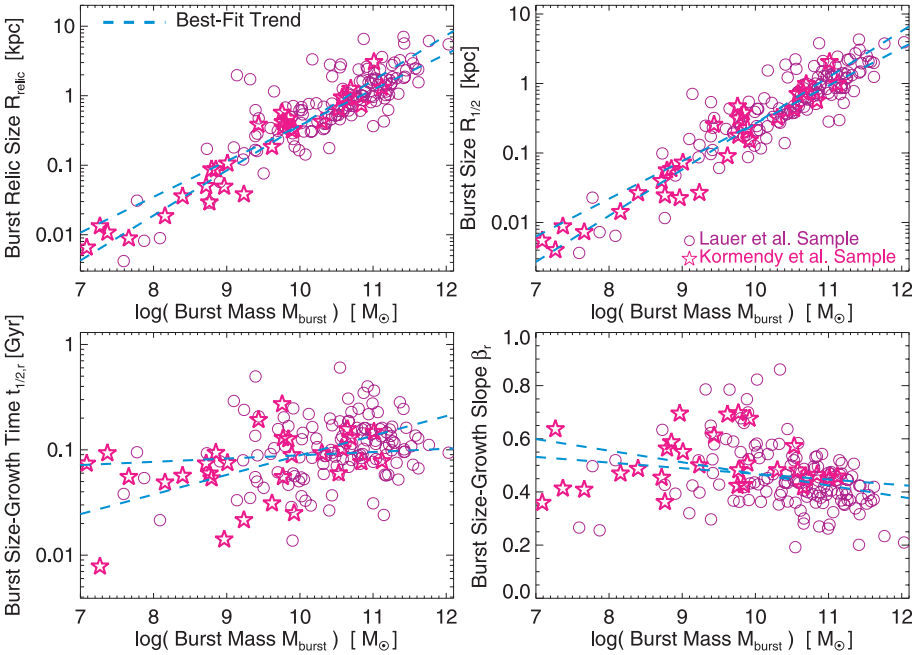

Figure 4. As Fig. 3 – observationally inferred properties of spheroid starbursts as a function of mass, from the relic starburst stars – but here giving the spatial size distribution of starbursts. Top left: size (projected half-stellar-mass radius) of the burst relics (generally a factor of ∼0.1 of the total galaxy size R_e), directly from the observed galaxy properties. Top right: size of the starburst at time $t = t_{1/2}$ (when the SFR is half-peak). The size here is defined as the half-SFR or half-light (assuming light traces SFR) radius; hence, it is more compact than the relic size. Bottom left: size-doubling time of the starburst (time for e.g. relative gas exhaustion in central, high-density regions to leave only star formation at larger radii, giving a larger apparent radius). This is simply related to the SFR decay time-scale in Fig. 3. Bottom right: best-fitting power-law slope to the increase of starburst scale radius versus time (equation 8).

mass and find a correlation of the form

$$R_{\rm relic} \approx 0.37\,{\rm kpc}\left(\frac{M_{\rm burst}}{10^{10}\,{\rm M}_\odot}\right)^{0.58} \quad (11)$$

with scatter $\sigma_{R_{\rm relic}} \approx 0.3$ dex. As a property of the *total* mass distribution, it is studied in more detail in H08c and H09b. There, it is shown that such sizes arise naturally from dissipational inflows, as a consequence of where the inflows stall and become self-gravitating. This is the reason that the power-law scaling in equation (11) reflects the observed scaling of spheroid sizes with mass (see e.g. Shen et al. 2003), and is a consequence of simple dynamics, independent of the star formation law.

Next, we consider $R_{\rm burst}$ (top right), the effective (half-*light*, assuming light traces local SFR) radius of the burst itself during the starburst episode (as shown in Fig. 2, bottom). For convenience, and as a reference point, we define the plotted quantity as $R_{\rm burst}(t_{1/2})$, i.e. the size at time $t = t_{1/2}$. This is a convenient parametrization and also has the advantage of being more representative of what might be observed, since the duty cycle at peak is vanishingly small. In any case, there is a similar correlation, with

$$R_{1/2} \equiv R_{\rm burst}(t_{1/2}) \approx 0.27\,{\rm kpc}\left(\frac{M_{\rm burst}}{10^{10}\,{\rm M}_\odot}\right)^{0.60} \quad (12)$$

with $\sigma_{R_{\rm relic}} \approx 0.3$ dex scatter.

As expected, the size $R_{\rm burst}$ near the peak of star formation is much smaller (by a typical factor ∼a few) than the size scale of the relic stars. This owes to two factors. First, near-peak, it is the highest density material just at the galaxy centre that dominates the SFR, while almost none of the more extended material is contributing at a significant level – hence the size of the burst itself will still grow by a large factor with time (see Fig. 2). Secondly, this size is weighted by the SFR, i.e. by gas density to some super-linear power according to the Kennicutt (1998) relation. If $\Sigma_{\rm gas}$ follows a Sersic law with some index n_s and effective radius R_e, and $\Sigma_{\rm SF} \propto \Sigma_{\rm gas}^{n_K}$, then it is trivial to show that the half-SFR radius will simply be $R_e \times n_K^{-n_s}$. For $n_s = 4$ and $n_K = 1.5$, this gives a factor of almost 5 smaller R_e for the SFR distribution (for $n_s = 2$, more typical of the inner components of the systems here, this is a more moderate factor of ∼2).

Nevertheless, the spatial sizes can still reach several kpc. In particular, for the *same* systems that reach $>1000\,{\rm M}_\odot\,{\rm yr}^{-1}$ peak SFRs, the effective radii are also large, ∼1–10 kpc. Moreover, we refer here only to the strict half-SFR radius; estimating an observed size in detail requires radiative transfer modelling. Analysis of simulations in Wuyts et al. (2009) and Wuyts et al. (in preparation), and similar analysis of some well-studied local starburst galaxies (Laine et al. 2003b), suggests that – especially at the peak of activity – the IR or radio size can be biased to factors of ∼2 larger than the true half-SFR radius owing to obscuration in the high-column-density nucleus and reprocessing of the emitted light.

Next, we consider the burst size-doubling time-scale, $t_{1/2,r}$. Unsurprisingly, the values are very similar to the SFR decay times $t_{1/2}$, with similar weak dependence on mass. We find a best-fitting median $t_{1/2,r}$:

$$t_{1/2,r} \approx 8.5\times10^{7}\,{\rm yr}\left(\frac{M_{\rm burst}}{10^{10}\,{\rm M}_\odot}\right)^{0.1}, \quad (13)$$

with a mass-independent scatter of $\sigma_{t_{1/2,r}} \approx 0.3$ dex.

We also consider the slope β_r of the starburst size versus time. Here, there may be a weak correlation with mass at the high-mass end, but formally this is only marginally significant (∼2σ) and only if we restrict ourselves to $M_{\rm burst} \sim 10^{10}$–$10^{12}\,{\rm M}_\odot$. We therefore

hesitate to quote a correlation, but do note the relatively robust median value of $\beta_r \sim 0.4$–0.5, with scatter $\sigma_{\beta_r} \approx 0.1$. Again, these naturally follow from the combination of profile shapes and the Kennicutt (1998) relation.

3.2.3 *Effects of a steeper Kennicutt–Schmidt relation*

Thus far, we have adopted the Kennicutt–Schmidt relation as calibrated at low redshifts (equation 2), with an index $n_K = 1.4(\dot{\Sigma}_* \propto \Sigma_{gas}^{n_K})$. However, some recent observations of high-redshift, massively star-forming systems have suggested that the SFRs of such systems exceed the predictions with this index and favour a somewhat steeper slope of $n_K = 1.7 \pm 0.1$ (Bouché et al. 2007). Specifically, they argue for a best-fitting relation

$$\dot{\Sigma}_* \approx 9.3 \times 10^{-5}\,M_\odot\,yr^{-1}\,kpc^{-2}\left(\frac{\Sigma_{gas}}{M_\odot\,pc^{-2}}\right)^{1.7}. \quad (14)$$

We caution that the high-redshift observations – in particular, the inferences of both gas masses and total bolometric luminosities and hence SFRs – remain uncertain. Nevertheless, this is an important source of error, and generally larger than many of the other systematic uncertainties (those being at the factor of an $\sim$2 level) in our modelling. Moreover, it can be particularly important in the most extreme systems, such as e.g. sub-millimetre galaxies, with high gas densities. We therefore re-consider our previous comparisons, but instead adopt this modified (steeper) index.

Table 2 shows the resulting revised fits, for quantities that are affected by this (e.g. the SFR and size versus time). The results are, in all cases, qualitatively very similar to those in Figs 2–4. We therefore show only the results of fitting the correlations and present a simple illustration of how the inferred burst properties change with n_K in Fig. 5. Specifically, we repeat our analysis of the observed Virgo systems from Fig. 2, but include both the previous results (with $n_K = 1.4$) and the steep-index results (with $n_K = 1.7$). For clarity, we show only a random subset of the observed systems. There are significant, systematic offsets between the implied star formation histories.

As expected, with a steeper index, i.e. larger SFR at high densities, the *peak* SFR of bursts is systematically higher. The difference is large – a factor of $\approx$5 higher peak SFR at fixed burst mass – giving $\langle \dot{M}_*(0) \rangle \approx 420\,M_\odot\,yr^{-1}\,(M_{burst}/10^{10}\,M_\odot)^{0.87}$; in other words, this implies that most systems with $M_{burst} > 3 \times 10^{10}\,M_\odot$ will exceed $1000\,M_\odot\,yr^{-1}$ SFRs at the peak of their starburst phase. However, with a higher SFR comes faster gas exhaustion, so the half-life of this peak, $t_{1/2}$, is systematically shorter, by a factor of $\approx$6 – i.e. typical exhaustion times of $t_{1/2} \approx 10^7$ yr. The decay slope β is also systematically different, now $\beta \approx 1.7$ (as opposed to 2.4 before) –

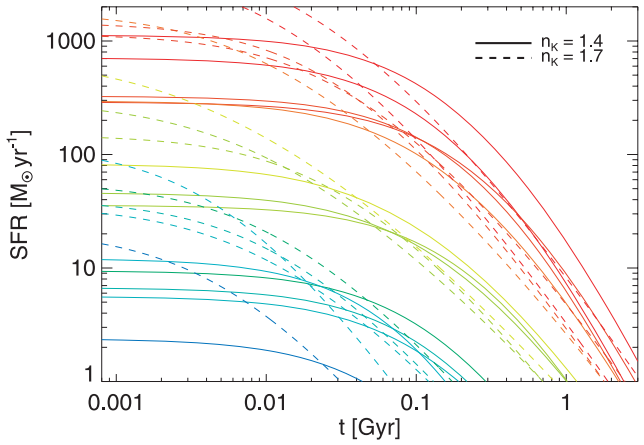

Figure 5. As Fig. 2 (middle), but comparing a subset of the inferred star formation histories from the observed systems with different assumed Kennicutt–Schmidt law indices. Solid lines, as Fig. 2, assume the $z = 0$ index, $n_K \approx 1.4$. Dashed lines assume a steeper relation suggested by some high-redshift observations, $n_K \approx 1.7$. The latter leads to more sharply peaked bursts with larger peak SFRs in early ($t < 10^8$ yr) stages. The star formation histories after $\sim$0.1 Gyr are similar, once gas surface densities have decayed to more moderate levels. Table 2 shows the results from re-fitting the correlations in Figs 3 and 4 with this higher $n_K = 1.7$.

this shallower power-law decay may appear counter-intuitive, but, from the form of equation (5), relates to the fact that the SFR at $t \ll t_{1/2}$ is more peaked with $n_K = 1.7$, and then at $t \gg t_{1/2}$ (when the gas density is lower) more extended (because the steeper index yields lower SFRs at low surface densities).

In practice, if one defines a starburst 'duration' by the time spent above some fixed, high SFR, this change in the Kennicutt–Schmidt slope does not actually have as dramatic an effect as implied by the change in $t_{1/2}$. At $t > 0.1$ Gyr, in fact, there is a relatively little difference in the SFR versus time, starting from the same observed relic starburst density profile (i.e. for the same relic object). Most of the difference comes at $t < 0.1$ Gyr. This is clear in Fig. 5.

3.3 Inferring the burst star formation history

3.3.1 *Methodology: the ages of bursts today*

Having quantified how burst properties scale with mass, and how these are connected to overall properties of their host galaxies, we require only a simple extension of our analysis to infer the cosmic history of starbursts.

Table 2. Starburst scaling relations with an alternative Kennicutt–Schmidt relation.

y	x	a	b	σ
$\log(\dot{M}_*[0]/M_\odot\,yr^{-1})$	$\log(M_{burst}/10^{10}\,M_\odot)$	2.62 ± 0.12	0.87 ± 0.11	0.35
$\log(t_{1/2}/Gyr)$	$\log(M_{burst}/10^{10}\,M_\odot)$	-1.97 ± 0.10	0.11 ± 0.09	0.30
$\log(\dot{M}_*[0])$	$\log(M_{burst}/t_{1/2})$	-0.38 ± 0.01	1.00 ± 0.01	0.06
β	$\log(M_{burst}/10^{10}\,M_\odot)$	1.69 ± 0.05	0.04 ± 0.04	0.22
$\log(R_{1/2}/kpc)$	$\log(M_{burst}/10^{10}\,M_\odot)$	-0.67 ± 0.07	0.61 ± 0.06	0.26
$\log(t_{1/2,\,r}/Gyr)$	$\log(M_{burst}/10^{10}\,M_\odot)$	-2.53 ± 0.23	0.06 ± 0.21	0.41
β_r	$\log(M_{burst}/10^{10}\,M_\odot)$	0.33 ± 0.01	-0.02 ± 0.01	0.08

Note. As Table 1, but adopting a Kennicutt–Schmidt star formation versus gas surface density relation with a steeper index ($\dot{\Sigma}_* \propto \Sigma_{gas}^{1.7}$), as suggested by observations of high-redshift, high-SFR systems.

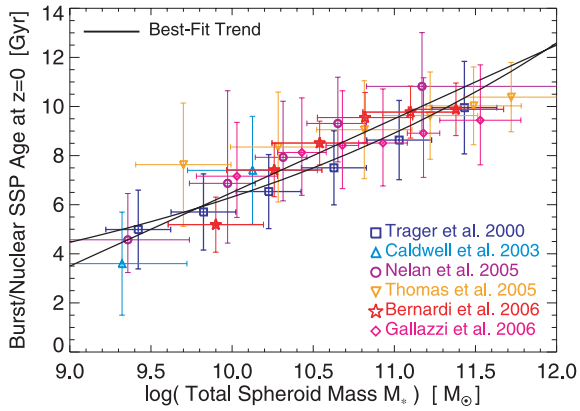

Figure 6. Observed average single stellar population age (at $z = 0$) of spheroid nuclear/most recent burst populations, as a function of the total spheroid stellar mass. Points show the median age at each mass from various determinations; error bars show the scatter (not the much smaller error in the mean). Observations are compiled from various sources (labelled). Solid black lines show the best-fitting log–log and log–linear trends for the median values (equation 15 and Table 1).

Fig. 6 shows the observed ages, at $z = 0$, of the dominant starburst in $z = 0$ ellipticals/spheroids as a function of their total stellar mass. We compile observations from a number of sources (Trager et al. 2000; Caldwell, Rose & Concannon 2003; Nelan et al. 2005; Thomas et al. 2005; Bernardi et al. 2006; Gallazzi et al. 2006); these involve various observational methodologies and selection functions, and together should plausibly represent the systematic uncertainties in this process. Note that for some of these samples, ages are quantified by environment; since the mass density of spheroids at the masses plotted is dominated by those in field environments, we show these values. Other observational estimates are within the scatter defined by these observations (e.g. Jørgensen et al. 1999; Kuntschner et al. 2001; Gallazzi et al. 2005). For each sample, the median age is well determined and agrees reasonably well with other estimates. A good approximation to the median ages is given by

$$t_{\rm lookback,\,burst} \approx 8.9\,{\rm Gyr}\left(\frac{M_*}{10^{11}\,{\rm M}_\odot}\right)^{0.15}. \quad (15)$$

We also plot the 1σ scatter in ages at each mass determined from each sample; these too agree well. We find that this is reasonably parametrized as a mass-independent, Gaussian ± 2 Gyr scatter.

Various analyses, e.g. observationally analysing mock SEDs constructed from hydrodynamic galaxy formation simulations or semi-analytic models of galaxy formation (see e.g. Trager & Somerville 2009, and references therein; Wuyts et al. 2009; Wuyts et al. in preparation), have shown that, for typical spheroids that combine stars formed over an extended (potentially still short in absolute terms) star formation history in pre-merger discs (assembled dissipationlessly in mergers) with stars formed in bursts via gas dissipation in mergers, these observed ages do reflect the cosmic time at which those bursts occurred. Since a number of constraints and theoretical models show that the time of last major gas-rich merger and time when star formation in 'quenched' systems must shut down are tightly coupled (even though there may not necessarily be a causal relationship between the two), this can also be thought of as dating the time of the last burst of star formation that consumed the residual gas in the systems (see Bundy et al. 2006, 2008; Cattaneo et al. 2006; Haiman, Jimenez & Bernardi 2007; Hopkins et al. 2006a, 2007, 2008b; Shankar, Bernardi & Haiman 2009). Moreover, most of these ages are derived specifically from the *central* stellar populations, those that are clearly formed dissipationally; thus they represent a clear constraint on when this burst occurred independent of more complex assembly and star formation histories for the more extended components. Finally, where available, detailed, resolved measurements of stellar population gradients show that these central populations do represent a distinct component, in agreement with dissipational models, and that their properties favour a single burst rather than an extended star formation history or dissipationless assembly of many distinct sub-components (Schweizer 1996; Titus et al. 1997; Schweizer & Seitzer 1998, 2007; Reichardt et al. 2001; Michard 2006).

Given these comparisons, it seems reasonable to take the age distributions in Fig. 6 as a first approximation to the times when these starbursts occurred. Together with the analytic fits to the distributions of burst properties versus mass, this enables us to reconstruct the burst history of the Universe. Specifically, we begin with the mass function of bulges/spheroids at $z = 0$, here adopting the determination in Bell et al. (2003). We ignore discs/late-type galaxies and very low-mass bulges, as these contribute negligibly to the quantities of interest (they have very low burst masses, hence low peak SFRs, where we will show that the population is dominated by non-burst star formation).[2] At a given mass, we know the number density of systems today and the distribution of burst masses $M_{\rm burst}(M_{*,\,\rm tot})$ (from e.g. equation 9, with appropriate scatter); that is, we know the (comoving) total number density of bursts with various masses that must have occurred before $z = 0$ to account for those systems. We also know the distribution of cosmic lookback times when those bursts happened, from equation (15) (again, with appropriate scatter). This allows us to construct a Monte Carlo population of bursts, each with some total mass and taking place (defined here as peaking) at some cosmic lookback time. Note that this is independent of the state of the remainder of the galaxy at this time – so is not affected if e.g. the outer portions of ellipticals are assembled much later (see e.g. Bezanson et al. 2009; Naab et al. 2009; Hopkins et al. 2009d,f,h).

We can then assign a full light curve to each burst, using the relations in Section 3.2 and Table 1, namely knowing the burst mass, a duration $t_{1/2}$ (equation 10) and power-law decay slope (median $\approx$2.4; again with scatter). Together, these define the corresponding peak SFR $\dot{M}_*(0)$. The time $t = 0$ in the light curve is simply the time of the burst, as determined above, and it evolves forwards from this time (the exact choice makes little difference, since the burst durations are small compared to the Hubble time). For convenience, we truncate each burst at a time $\approx 20\,t_{1/2}$, but by this point the luminosity has decayed sufficiently that the burst is negligible. We then make mock observation of the Monte Carlo population at any redshift z and construct the LF or luminosity density of bursts. Of course, we are really predicting a distribution of SFRs; for comparison with observations, we convert these to total (8–1000 μm)

[2] We have experimented with alternative determinations of the bulge-dominated galaxy mass function at $z = 0$, including those presented in Bernardi et al. (2009) and Vika et al. (2009). We have also attempted to construct the mass function of bulges specifically, following Driver et al. (2007) or by adopting the morphology-separated mass functions from Kochanek et al. (2001) with a type-dependent B/T from Balcells, Graham & Peletier (2007b). We find that these make little difference to any of our conclusions, as the resulting differences lie primarily in identification of low-mass bulges or bulges in late-type galaxies which are negligible in the total IR luminosity density.

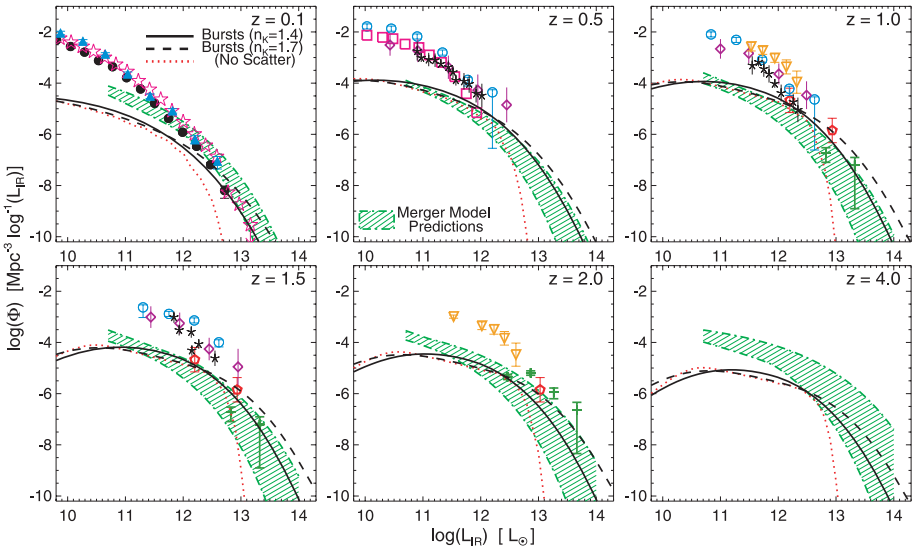

Figure 7. Total (8–1000 μm) IR LFs as a function of redshift. We show the contribution from bursts, using the methodology presented here (black lines), assuming a Kennicutt–Schmidt index of $n_K = 1.4$ (solid) or 1.7 (dashed). The dotted red line shows the result neglecting the scatter in the correlations shown in Figs 3 and 4; including the observed dispersion is important to explain rare, extreme starbursts. Points show observed estimates from Saunders et al. (1990, magenta stars), Soifer & Neugebauer (1991, blue triangles), Yun et al. (2001, black filled circles), Huang et al. (2007, magenta squares), Le Floc'h et al. (2005, violet diamonds), Caputi et al. (2007, orange inverted triangles), Magnelli et al. (2009, black $*$), Babbedge et al. (2006, red pentagons),Chapman et al. (2005, dark green $+$) and Pérez-González et al. (2005, blue open circles). The shaded green range shows the prediction (with systematic uncertainty) for the IR LF of merger-induced bursts from the semi-empirical models and hydrodynamic simulations in Hopkins et al. (in preparation).[4] The burst contribution dominates the bright end of the IR LF, agreeing well with predicted merger-induced bursts and other constraints, but is a small fraction of the typical $\sim L_*$ activity at any redshift. The luminosity threshold above which bursts are important increases with redshift, along with the entire LF. Fits to the burst LF inferred here are provided in Table 3.

IR luminosities with the empirically calibrated conversion factor in equation (4).[3]

We can also trivially repeat this procedure for a different bolometric correction from $\dot{M}_*$ to L_{IR} (which will systematically shift the predicted luminosities by some factor of $\sim$2). Likewise, we can repeat our calculation using the fitted scaling relations appropriate for a steeper Kennicutt–Schmidt law with index $n_K \approx 1.7$ rather than $n_K \approx 1.4$, given in Table 2.

3.3.2 *The luminosity function of bursts*

Fig. 7 shows the resulting burst LFs at a variety of redshifts from $z = 0$–4. We compare with observations compiled from a number of sources, available from $z \sim 0$–3. Note that all of these are corrected to a total IR luminosity from observations in some band; we adopt the corrections compiled in Valiante et al. (2009), but emphasize that some caution, and at least a systematic factor of $\sim$2 uncertainty in L_{IR}, should be considered in estimates from most if not all observed wavelengths.

At low luminosities, the predicted LFs are well below those observed, but they grow rapidly in importance, and are roughly consistent with the observations, at the high-luminosity end. This is expected –it is well established that star formation at relatively low rates is dominated by quiescent star formation in normal (e.g. non-merging) galaxies, i.e. distributed star formation in discs rather than dissipational starbursts (see e.g. Sanders & Mirabel 1996; Bell et al. 2005; Sajina et al. 2007; Noeske et al. 2007a,b; Tacconi et al. 2008; Jogee et al. 2009; Robaina et al. 2009; Veilleux et al. 2009). At low redshifts, for example, nuclear starbursts (typically merger-induced) are negligible at luminosities of $\lesssim 10^{11}\,L_\odot$, but at the highest luminosities, $>10^{12}\,L_\odot$, they become dominant (Sanders & Mirabel 1996). At higher redshifts, the LF of bursts increases rapidly, as does the global LF. This is again expected, as increasing gas fractions and specific SFRs lead all systems (mergers and quiescent discs) to higher SFRs at fixed mass. Thus, at *all* redshifts the (relatively) low-luminosity population remains non-burst-dominated, and the threshold (in terms of L_{IR}) for burst domination moves up to higher luminosities ($L_{IR} \gtrsim 10^{12}\,L_\odot$ at $z \sim 1$ and $L_{IR} \gtrsim 10^{13}\,L_\odot$ at $z \sim 2$). In terms of space densities, the burst population becomes important at $\sim 10^{-5}\,\mathrm{Mpc^{-3}\,log^{-1}}\,L_{IR}$, with much weaker redshift dependence. This is similar to the behaviour predicted in models of merger-induced star formation bursts (Hopkins et al. 2009j).

We show predictions for both the cases of the low-redshift Kennicutt–Schmidt law slope of $n_K \approx 1.4$ and the suggested steeper value of $n_K \approx 1.7$ from high-redshift observations. Unsurprisingly, assuming a steeper relationship implies more intense SFRs at the peak of activity, so the predicted burst LF extends to higher luminosities. However, the shorter gas exhaustion time means that there is a lower number density at low/intermediate luminosities. The difference is clearly non-trivial, given the rarity of the highest luminosity sources. The results in the steep-index case are comparable, however, to those obtained from the shallow-index case if we were to assume that the scatter in the relevant quantities is systematically larger by $\sim$0.1 dex – in other words, this continues

[3] Note that, in comparing to observed starburst light curves or LFs, the average M_*/L will depend systematically on the IMF. However, the inferred stellar surface mass density on which we base our analysis is determined from observed luminosity profiles, with the same systematic dependence on M_*/L. Thus, so long as the IMF does not evolve with redshift, variations between typical choices make little difference.

the same trends, and the effects may be comparable in magnitude to other uncertainties discussed here.

We also provide simple fits to the inferred LF of bursts, as a function of redshift, for both the shallow and steep Kennicutt–Schmidt slopes. Following standard convention, we fit the LF with a double power-law form:

$$\Phi \equiv \frac{\mathrm{d}n}{\mathrm{d}\log L} = \frac{\phi_*}{(L/L_*)^{\alpha} + (L/L_*)^{\gamma}}, \tag{16}$$

where the parameters ϕ_* (normalization), L_* (break luminosity), α (faint-end slope, i.e. $\Phi \propto L^{-\alpha}$ for $L \ll L_*$) and γ (bright-end slope, i.e. $\Phi \propto L^{-\gamma}$ for $L \gg L_*$) depend on redshift, with that dependence conveniently approximated as

$$\begin{aligned} \log L_* &= L_0 + L'\,\xi + L''\,\xi^2 \\ \log \phi_* &= \phi_0 + \phi'\,\xi + \phi''\,\xi^2 \\ \alpha &= \alpha_0 + \alpha'\,\xi + \alpha''\,\xi^2 \\ \gamma &= \gamma_0 + \gamma'\,\xi + \gamma''\,\xi^2 \\ \xi &\equiv \log(1+z). \end{aligned} \tag{17}$$

(Note that log here and throughout refers to $\log_{10}$.) We perform this fit using our results only up to redshift $z = 4$, as the uncertainties grow rapidly at higher redshift. The fits should be considered with caution at higher redshifts. We provide the best-fitting parameters in Table 3, along with their uncertainties.

We briefly note that, especially because bursts are important at the high-luminosity end of the total LF, incorporating the scatter in the relevant relationships in Section 3.2 is critical to the predicted abundance of IR-bright systems. In Fig. 7, we compare the prediction if we were to ignore all scatter – i.e. simply construct our Monte Carlo population using just the median values of all parameters and their correlations. As expected, this cuts off much more quickly at the high-luminosity end, reflecting the rapid exponential cut-off in the observed number of high-mass galaxies.

Recently, Hopkins et al. (in preparation) presented predictions from galaxy formation models for the contribution to the SFR and IR luminosity distributions from normal, quiescent star-forming galaxies, from merger-induced bursts of star formation and from active galactic nuclei (AGN). The models used a halo-occupation-based approach in order to populate galaxies at each redshift (i.e. simply beginning with observed galaxy stellar mass functions and gas masses, with merger rates determined from evolving this forwards in agreement with observed merger fractions) and then mapping each population to suites of high-resolution simulations, to predict the distribution of SFRs in various systems. We compare their predictions for the merger-induced starburst population to our inferred burst SFR and IR luminosity distributions in Fig. 7.[4] Given the systematic uncertainties they quote (shown as the shaded range in the figure), and ours here, the agreement is reasonable. The two diverge at $z \gg 3$, but this is where the uncertainties in both the modelling and our empirical inferences become large. The faint-end extrapolations are also different, but in neither case are these well constrained (in a systematic sense, at very low SFR/late times, the designation as 'burst' is somewhat arbitrary). In general, the agreement seen supports our interpretation of the burst components of galaxies and

[4] The merger rates determined in this model are presented in Hopkins et al. (2009i). A 'merger rate calculator' script to give the merger rate as a function of galaxy mass, mass ratio and gas fraction, which determines these LFs, is publicly available at http://www.cfa.harvard.edu/~phopkins/Site/mergercalc.html.

Table 3. Fits to IR LF of bursts.

$L_0(\pm\,\Delta L_0)^a$	L'^b	L''^c	$\phi_0{}^d$	ϕ'^e	ϕ''^f	$\alpha_0{}^g$	α''^h	α''^i	$\gamma_0{}^j$	γ'^k	γ''^l
Double power-law fit – Standard Model[m]											
11.87(0.09)	5.08(0.43)	−7.29(0.48)	−6.29(0.17)	3.76(0.85)	−2.48(0.94)	0.98(0.09)	0.39(0.49)	−3.33(0.62)	2.68(0.16)	7.13(0.82)	−11.38(0.94)
Double power-law fit – steeper Kennicutt–Schmidt index[n]											
11.89(0.09)	6.75(0.44)	−9.08(0.51)	−6.27(0.15)	1.47(0.78)	−0.15(0.90)	0.87(0.07)	0.63(0.40)	−2.63(0.49)	2.29(0.12)	8.11(0.70)	−12.32(0.84)

Note. Parameters are given for best fit to the redshift-dependent form of the IR LF (equations 16 and 17): $\Phi(z) = \phi_*/[(L/L_*)^{\alpha} + (L/L_*)^{\gamma}]$.
[a–c]Break luminosity L_* as a function of redshift, per equation (17): $\log\{L_*/L_{\odot}\} = L_0 + L'\,\xi + L''\,\xi^2$, where $\xi \equiv \log(1+z)$.
[d–f]Normalization ϕ_*: $\log\{\phi_*/\mathrm{Mpc}^{-3}\log^{-1} L_{\mathrm{IR}}\} = \phi_0 + \phi'\,\xi + \phi''\,\xi^2$ [g–i]Faint-end slope α: $\alpha = \alpha_0 + \alpha'\,\xi + \alpha''\,\xi^2$.
[j–l]Bright-end slope γ: $\gamma = \gamma_0 + \gamma'\,\xi + \gamma''\,\xi^2$.
[m]LFs assuming the low-redshift fitted slope for the Kennicutt–Schmidt relation between star formation and gas surface density, $n_{\mathrm{K}} = 1.4$.
[n]Same, assuming instead the steeper slope suggested by high-redshift observations, $n_{\mathrm{K}} = 1.7$. All fits are based on $z = 0$– 4 results. Extrapolation beyond these redshifts should be performed with caution. Statistical uncertainties in the fitted parameters are given in parentheses.

favours a possible merger origin for these bursts. More important, the burst history inferred here should *not* correspond to the normal or quiescent star-forming population.

3.3.3 The problem of bright sub-millimeter galaxies (SMGs)

We also note that, at $z \sim 2$–3, our reconstruction appears to somewhat underpredict the abundance of the most luminous starburst systems relative to observations. However, at this redshift, the only constraints at the high luminosities of interest come from the sub-millimetre populations observed in Chapman et al. (2005). This is a relatively small sample, with a number of difficult completeness corrections involved in estimating the number density, and non-trivial cosmic variance given the sample selection. Recently, analyses of the number counts of similarly bright sources in much larger IR surveys have suggested that the average counts may actually be much lower – a factor of $\sim$5 difference (with higher estimates owing to substantial cosmic variance; see e.g. Austermann et al. 2009).

Perhaps more important, given that the number densities in this regime fall rapidly with $L_{\rm IR}$, a small error in the bolometric correction translates to order-of-magnitude differences in number density at fixed L. And indeed, such a conversion from the sub-millimetre to the total IR flux is highly uncertain, depending on quantities that are not well known for these populations, such as the dust temperature, and subject to large object-to-object variation in the local Universe. It should also be stressed that the observed high-redshift points in Fig. 7 have not been corrected for possible AGN contributions to the IR luminosity, although (from indirect constraints) it has been argued that AGN are unlikely to contribute more than $\sim$30 per cent of the bolometric luminosity in these systems (Bussmann et al. 2009; Casey et al. 2009; Menéndez-Delmestre et al. 2009). For these reasons, we consider the comparison at these redshifts and luminosities to be largely qualitative. A more detailed comparison would require full modelling from e.g. high-resolution simulations that include spatially dependent, multiphase star formation, metallicity, gas and dust distributions that can forward-model the full spectral energy distribution (SED) of such bursts (for some preliminary such results, we refer to Li et al. 2008; Jonsson, Groves & Cox 2009; Narayanan et al. 2009a,b; Younger et al. 2009).

But the comparison in Fig. 7 emphasizes an important point: *if* the number density and bolometric corrections of such high-luminosity systems are correct, then either the Kennicutt (1998) law must break down severely at high redshifts (giving much higher SFRs than implied by e.g. observations of high-density systems in Bouché et al. 2007, at fixed surface density) or something must be fundamentally wrong in our conversion between mass and light, either at low redshifts (i.e. some dramatic errors in measurements of the surface brightness and stellar masses of local ellipticals, which appear unlikely) or at high redshifts (i.e. the results of a strongly time-dependent stellar IMF or large heavily obscured AGN contributions to the high-z luminosities).

Taken at face value, the number density of high-z bursts inferred, coupled with their implied SFRs, would imply far too much high-density material in massive systems today. All of our analyses of burst SFRs effectively set an upper limit on the burst number density at high-L. Consider, for example, the consequences of relaxing our assumptions. If starbursts were split into several separate events, with lower initial burst rates, then the duty cycle would go up, but the absolute L would go down (and in this portion of the LF, the net result would be a severe decrease in the high-$L_{\rm IR}$ prediction). If systems were not initially gas-dominated or 100 per cent gas, but maintained some lower gas fraction in a quasi-steady state for the time needed to build up their densities, then again the peak luminosities decrease severely. If the present-day densities are the result of assembling many systems, then this is the same as breaking up bursts, and leads to a lower prediction. The bursts cannot be more concentrated in time (yielding a higher peak SFR) without violating the Kennicutt (1998) law; even doing so, they become more luminous but shorter, and it requires an order-of-magnitude change to the star formation relation before this yields a match.

Ultimately, a number of other obvious comparisons make this clear. Yielding the implied SFRs of the observed bright SMG systems (taken at face value) without breaking the Kennicutt (1998) relation requires $\sim 10^{11}\,{\rm M_\odot\,kpc^{-2}}$ gas (and ultimately stellar) surface densities, over spatial radii of $\sim$1–2 kpc. Although this is indeed comparable to the highest stellar surface densities in ellipticals, observed systems only reach those surface densities at $\lesssim$100 pc scales, *not* at kpc scales (where the typical surface density in a massive elliptical is $\approx 10^{10}\,{\rm M_\odot\,kpc^{-2}}$). Also, given the characteristic SMG lifetime of $\sim 10^8$ yr, from observational constraints, it is straightforward to estimate the total amount of stellar mass that would be formed at or above these surface densities, from SMGs over the redshift range $z \sim 2$–4, and the number comes to $\sim 10^8\,{\rm M_\odot\,Mpc^{-3}}$ [$\Sigma_* > 10^{11}\,{\rm M_\odot\,kpc^{-2}}$]. Hopkins et al. (2009a) calculate the actual observed stellar mass density in all galaxies above such a threshold and find that it is $\approx 1.5 \times 10^6\,{\rm M_\odot\,Mpc^{-3}}$, well below the range of uncertainties owing to e.g. stellar mass loss and the somewhat uncertain values above.

3.3.4 The burst luminosity density

Fig. 8 integrates the LFs shown in Fig. 7 to give the total IR luminosity density and corresponding total SFR density, owing to bursts, as a function of redshift. Note that many of the uncertainties that might affect our other results are integrated out here (e.g. the exact light curve shape or Kennicutt–Schmidt slope). We compare with the total SFR density from a number of observations in IR, radio and UV wavelengths as compiled in Hopkins & Beacom (2006), as well as that inferred at high redshifts from observations of the Lyman α forest in quasar spectra and implied ionizing background, compiled in Faucher-Giguère et al. (2008). As expected from Fig. 7, the predicted SFR density owing to bursts is well below the total SFR density observed. This clearly demonstrates that bursts do not, and cannot, dominate the total SFR density.

We compare with a number of observations that attempt to estimate the luminosity or SFR density induced by mergers. First, we stress that this is different from the *total* SFR density in objects *identified as* mergers. A merger can take $\sim$2 Gyr to complete, but the SFR over most of that time will simply reflect that of the quiescent discs, with at most a modest enhancement. The burst itself, where gas dissipation drives inflows into the centre of the merger remnant, enhancing the SFR significantly, has a duration of only $\sim$0.1 Gyr. Nevertheless, using statistical samples of mergers and non-merging systems, and comparing their SFR distributions, various authors have attempted such a comparison.[5]

[5] Note that most of these authors actually measure the *fraction* of the SFR density in or induced by mergers, not the absolute value. We convert this to an absolute density by rescaling with the observed total SFR density at the same redshift from the best-fitting observed trend presented in Hopkins & Beacom (2006).

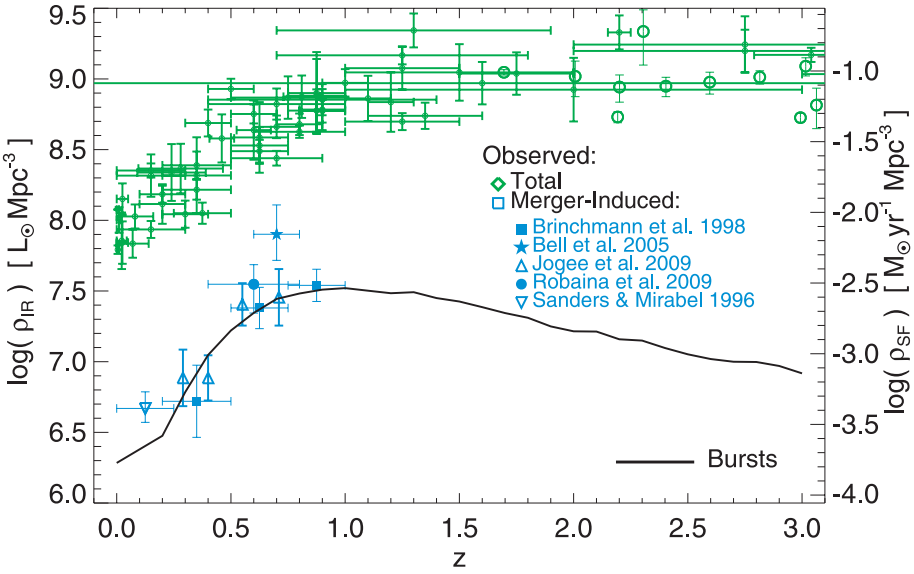

Figure 8. Total IR luminosity density (and corresponding SFR density) as a function of redshift. We show the inferred contribution owing to bursts (solid black line) from the observed $z = 0$ spheroid properties. We compare the observational compilation from Hopkins & Beacom (2006) for the *total* IR luminosity density/SFR density (green diamonds), and at high redshifts the SFR density inferred from Lyman α forest measurements in Faucher-Giguère et al. (2008, green circles). We also compare observed estimates of the SFR density induced in mergers (blue points), from Jogee et al. (2009, triangles), Sanders & Mirabel (1996, inverted triangle), Robaina et al. (2009, circle), Brinchmann et al. (1998, squares) and Bell et al. (2005, star). The burst component of star formation is a small fraction of ∼5– 10 per cent of the total IR luminosity density (most stars are formed quiescently in discs and are then violently relaxed into spheroids). This agrees well with observational estimates of the fraction of star formation owing specifically to mergers, as predicted if these mergers induce the angular momentum loss that drives gas dissipation in forming spheroids.

Typically, in these cases, the SFR density of some merger sample (identified in a similar manner) is considered, but only after subtracting away the expected contribution from quiescent star formation. In general, this is accomplished via comparison to some control sample of star-forming galaxies with similar stellar masses and at comparable redshifts. Robaina et al. (2009) attempt this from a pair-selected sample at $z \sim 0.4$–0.8; Jogee et al. (2009) perform such an estimate from morphologically selected galaxies at $z \sim 0.4$–1. We also compare with somewhat less well-defined, but similar samples that estimate the total amount of star formation in observationally identified ongoing mergers or recent (morphologically disturbed) merger remnants. We compile observations from Brinchmann et al. (1998) and Bell et al. (2005), who estimate this quantity in morphologically selected objects at $z \sim 0$–1.5. We perform a similar exercise at low redshift using the fraction of late-stage major merger systems as a function of IR luminosity from Sanders & Mirabel (1996), together with the IR LFs from Saunders et al. (1990) and Yun, Reddy & Condon (2001), to estimate the fraction of the luminosity density in mergers. Because the selection of ongoing mergers is somewhat strict in these samples (isolating near-peak times), they are not very different from the estimates of merger-induced star formation, but formally should still be considered upper limits.

Our prediction agrees well with these observations, over the range $z = 0$–1. In fact, given the (probable factor of ∼2) systematic uncertainties involved in both, the level of agreement is surprising and may be somewhat coincidental. But, in general, both direct estimates and our indirect constraint imply that bursts constitute ∼5–10 per cent of the SFR density and that this is not dramatically larger at high redshifts. The agreement here also provides further evidence that most of the bright, massive bursts of interest here are really merger-induced, since that is specifically what is observed. If there were a large non-merger population, the observations should be much lower than our prediction.

We have also compared both to the predictions of the most recent generation of cosmological models. Somerville et al. (2008) use semi-analytic models and Hopkins et al. (2008d, 2009g) employ semi-empirical (halo-occupation-based models), both combined with the predictions from high-resolution galaxy merger simulations (Cox et al. 2008; Hopkins et al. 2009c) to predict the merger-induced burst SFR and luminosity density as a function of redshift. Most recently, Hopkins et al. (in preparation) present a revised version of these semi-empirical models based on larger suites of simulations and improved halo-occupation constraints and modelling, and specifically present fits to the merger-induced burst population. These are compared to our predicted LFs in Fig. 7. Comparing all of these results to our predictions in Fig. 8, we find good agreement (unsurprising, given that the predicted LFs in Fig. 7 also agree well). The important point is that most recent models also predict that only ∼5–10 per cent of the SFR density come from mergers, at all redshifts.

Finally, we hesitate to extrapolate our results beyond $z \sim 2$–3, for two primary reasons. First, because the Hubble time is short at higher redshifts, the predictions become sensitive to ∼0.1–1 Gyr systematic uncertainties in stellar population age estimates, which are known to be problematic particularly in the old-age regime. Secondly, the higher in redshift we consider, the more likely we are to see effects of differences between star formation and assembly histories, even for the bursts themselves (where, at least at low redshifts, observations suggest that the two are tightly coupled; that is, bursts tend to be dominated by a single most massive burst, rather than many smaller sub-components). We therefore caution against the over-interpretation or extrapolation of our results at $z \gtrsim 4$.

4 DISCUSSION

It has long been believed that the centres of galaxy spheroids must be formed in dissipational starburst events, such that gas in the outer parts of a galaxy must lose angular momentum rapidly and fall in on roughly a dynamical time to the galaxy centre. Recently, observations have shown that it is possible to robustly separate the 'burst' component of galaxy profiles from the outer, violently relaxed component owing to the scattering of progenitor galaxy stars formed over earlier, more extended periods. As detailed, high-resolution observations of e.g. spheroid stellar mass profiles, shapes, kinematics and stellar population properties improve, such decompositions become increasingly robust and applicable to a wide range of systems.

In this paper, we use these observations as a novel, independent constraint on the nature of galactic starbursts. We stress that by 'starburst' here, we do *not* mean simply any high-SFR system; rather, we refer specifically to star formation in central, usually sub-kpc scale bursts owing to large central gas concentrations driven by angular momentum loss as described above. These are commonly associated with galaxy–galaxy mergers, which have long been known to efficiently drive starbursts and violent relaxation (e.g. Lynden-Bell 1967; Toomre 1977; Barnes & Hernquist 1991, 1996; Mihos & Hernquist 1994, 1996; Barnes 1998). But they could also owe to any other sufficiently violent process, e.g. gas inflows owing to disc bars or during dissipational collapse.

Regardless of origin, we can robustly identify the starburst relics and stellar mass surface density profiles in well-observed spheroids at $z = 0$. This methodology and tests of its accuracy have been discussed in Hopkins et al. (2008a), H08c, H09b and H09e. This alone is a powerful integral constraint on the star formation histories of these systems. But we show that they can in fact be used to provide more detailed information, by allowing for the inversion and recovery of the star formation history of each burst. We can thus use local observations to recover the full time-dependent and scale-dependent star formation history of each burst, if we couple these observed constraints to simple, well-motivated assumptions, namely some form of the Kennicutt–Schmidt relation (between the SFR and gas surface density) applied in the formation of these stars and they formed in dissipational (i.e. rapid and initially gas-rich, on these scales) events. Both assumptions are directly motivated by observations, but we also consider how uncertainties in them translate into uncertainties in the resulting constraints.

Performing this exercise, we recover a large number of empirically determined parameters of starbursts and quantify how they scale as a function of mass and other properties. This includes the total mass of the starburst and the time-dependent SFR. In general, we find that the constrained starbursts can be reasonably well approximated by a simple power-law behaviour (equation 5), rising and decaying from a characteristic maximum SFR with characteristic half-life $t_{\rm burst}$ and a typical late-time power-law slope of $\dot{M}_* \propto (t/t_{\rm burst})^{-\beta}$ where $\beta \sim 2.0$–3.0.

The characteristic burst mass $M_{\rm burst}$ is $\sim$10 per cent of the total spheroid mass, but it scales weakly with galaxy mass in a manner similar to how disc galaxy gas fractions scale with their stellar masses (expected if discs are the pre-merger progenitors of spheroids), $M_{\rm burst} \approx 1/(1 + [M_*/10^{9.15}\,{\rm M}_\odot]^{0.4})$. Detailed discussion of this trend, and its consequences for the global structure and kinematics of spheroids, are presented in Hopkins et al. (2008a). However, this already makes it clear that bursts should not dominate the SFR density. They are a small fraction of $\sim$10 per cent of all stars in spheroids (let alone all stars). That does not mean that bursts are unimportant, however. It is clear that they control many of the properties of galaxies (Cox et al. 2006; Naab et al. 2006; Oñorbe et al. 2006; Robertson et al. 2006; Ciotti, Lanzoni & Volonteri 2007; Jesseit et al. 2007; Jesseit et al. 2009; Covington et al. 2008; H09b; H09e), and they can account for the short-lived, highest-SFR systems in the Universe. Moreover, the scatter in burst mass is significant, $\sim$0.3–0.4 dex, which is critical for explaining the most extreme starbursts in the Universe, which require both large absolute galaxy masses and gas fractions to reach the very high burst masses required.

The typical starburst time-scale implied from the combination of observed surface densities and the Kennicutt (1998) law is a nearly galaxy-mass-independent $t_{\rm burst} \sim 10^8$ yr. Both the value of this time-scale and the weak scaling with galaxy and/or burst mass agree well with the dynamical times in the central $\sim$kpc of galaxies. As above, though, there is considerable scatter of the order of $\sim$0.2 dex. Given such a short starburst time-scale, and the relatively small total mass fractions involved in starbursts, it naturally follows that starbursts will represent only a small fraction of the star-forming galaxies at any stellar mass, at a particular instant. Given that the average number of bursts per galaxy is not large, the duty cycle of bursts should be $\sim t_{\rm burst}/t_{\rm Hubble}$, or $\sim$1–5 per cent from $z = 0$–3. Indeed, observations have shown that most galaxies at these redshifts lie on a normal star-forming sequence, without a large $\sim 1\sigma$ scatter from e.g. merger-induced bursts (Bell et al. 2005; Papovich et al. 2006; Noeske et al. 2007a,b). The small duty cycle here means that even if the burst SFR enhancement is large, it will not violate these constraints (appearing only at the $\sim$2–3σ level in the wings of the SFR distribution at a given mass).

These conclusions are supported by independent evidence from observational stellar population synthesis studies. Specific comparisons to the objects considered here, where available, are presented in detail in H09b, H09e and Foster et al. (2009). It is well established that constraints from abundances require that the central portions of spheroids be formed in a similar, short time-scale. And detailed decomposition of stellar populations into burst plus older stellar populations have yielded consistent results for the typical burst fractions and sizes (Titus et al. 1997; Schweizer & Seitzer 1998; Reichardt et al. 2001; Michard 2006).

As should be expected from the generic behaviour above, bursts peak at SFRs of $\sim M_{\rm burst}/t_{\rm burst}$, which follows $M_{\rm burst}$ (and hence total spheroid mass) in a close-to-linear relation. The most massive local ellipticals – especially those with total stellar masses of $\gtrsim 10^{12}\,{\rm M}_\odot$ – had extreme peak SFRs of $>1000\,{\rm M}_\odot\,{\rm yr}^{-1}$. Thus, it is at least possible that some local systems reached the highest SFRs inferred for massive, high-redshift starburst galaxies (Chapman et al. 2005; Papovich et al. 2005; Walter et al. 2009). More moderate, but still massive ellipticals with $M_* \sim 1$–$5 \times 10^{11}\,{\rm M}_\odot$ reached a range of peak SFRs from $\sim$30 to $500\,{\rm M}_\odot\,{\rm yr}^{-1}$, corresponding to their forming fractions from $\sim$5–20 per cent of their total masses in starbursts. These match well with the observed SFRs in more typical, local and $z \sim 1$ starbursts (in $\sim L_*$ galaxies), which have been specifically associated with mergers driving gas to galaxy centres and forming the appropriate nuclear mass concentrations to explain e.g. elliptical kinematics, sizes, phase-space densities and fundamental plane scalings (Cox et al. 2006; Naab et al. 2006; Robertson et al. 2006; Hopkins et al. 2008a, 2009d; H08c; Jesseit et al. 2009).

We similarly quantify starburst spatial sizes as a function of their mass, peak SFR and time. Starburst sizes scale with starburst mass in a similar fashion as the spheroid mass–size relation, but are smaller than their host spheroids by a fraction similar to their mass fraction.

The most massive starbursts reach half-SFR (i.e. half-light, in IR or millimetre wavelengths) size scales of ∼1–5 kpc. For typical spatial distributions, this implies total spatial extents of a strong emission of up to ∼10 kpc. These size scales also agree well with observations of the most massive high-redshift starbursting systems (Tacconi et al. 2006; Schinnerer et al. 2008; Younger et al. 2008) and of massive, compact ellipticals formed at high redshift, believed to be the relics of such starbursts (with, at that time, little envelope of dissipationless, low-density material yet accreted; Trujillo et al. 2006; Cimatti et al. 2008; van Dokkum et al. 2008; Bezanson et al. 2009; Hopkins et al. 2009h).

For more typical, $\sim L_*$ starbursts, sizes range from ∼0.1 to 1 kpc, also similar to those observed in merging systems (Scoville et al. 1986; Sanders et al. 1988; Hibbard & Yun 1999; Tacconi et al. 2002; Laine et al. 2003b; Rothberg & Joseph 2004). The size difference between these and the most extreme objects follows from the much larger gas supply involved – there is no dramatic difference in the relic starburst mass distribution *shapes*. Some claims have been made that the large sizes of high-redshift starbursts could imply that they are not scaled-up analogues of local extreme starbursts, but we find here that they correspond naturally. Scaling up a starbursting system in the starburst mass fraction will not preserve spatial size, but rather will scale along the starburst size–mass relation here, which appears to be smooth and continuous from the smallest starbursts with masses of $\sim 10^7\,M_\odot$ to the largest with masses of $>10^{11}\,M_\odot$. The origin of the size–mass scaling is of considerable physical interest. It has been proposed that in such starbursts the Eddington limit from radiation pressure on dusty gas sets a universal maximum central surface density, over all mass scales, from which this follows (Hopkins et al. 2009f). The important constraint, from our analysis, is that there is no discontinuity, and we provide the scaling relations that any such model must satisfy.

Combining these constraints with observational measurements of the nuclear stellar population ages of these systems – i.e. the distribution of times when these bursts occurred – we show that it is possible to re-construct the dissipational burst contribution to the distribution of SFRs and IR LFs and luminosity density of the Universe. We show that the burst LFs agree well with the observed IR LFs at the brightest luminosities, at redshifts $z \sim 0$–2. At low luminosities, however, bursts are always unimportant, as expected from their short duty cycles, noted above. Although the burst LFs rise with redshift, they always represent low space densities, and the overall LF evolves rapidly. As such, the transition luminosity above which bursts dominate the IR LFs and SFR distributions increases with redshift from the ULIRG threshold at $z \sim 0$ to HyLIRG thresholds at $z \sim 2$. This appears to agree well with recent estimates of the transition between normal star formation and mergers, along the observed LFs. Systematic morphological studies at low redshifts (Sanders & Mirabel 1996) yield the conventional wisdom that – locally – the brightest LIRGs and essentially all ULIRGs are merging systems (see also references in Section 1). At high redshifts, similar studies have now been performed (see e.g. Tacconi et al. 2008, and references therein). They too find that the brightest sources are almost exclusively mergers, but with a transition point an order-of-magnitude higher in luminosity. Other morphological studies at intermediate redshifts $z \sim 0.4$–1.4 have reached similar conclusions (Bridge et al. 2007).

Integrating these LFs, we find the burst contribution to the SFR and IR luminosity densities of the Universe and show that it is small at all redshifts, rising from ∼1–5 per cent at $z \sim 0$ to a roughly constant ∼4–10 per cent at $z > 1$. This agrees well with recent attempts to estimate the contribution to the SFR density at $z = 0$–1 specifically from merger-induced starbursts, using either pair or morphologically selected samples (Jogee et al. 2009; Robaina et al. 2009).[6] Given the completely independent nature of the constraints, and significant uncertainties involved in both, the agreement is good. The small value is what is expected, given our previous determination that the typical burst mass is just ∼10 per cent in $\sim L_*$ spheroids (the galaxies that dominate the stellar mass density). But it clearly rules out merger-induced bursts driving the SFR density evolution of the Universe.

At the highest redshifts $z \gtrsim 2$, we can put strict upper limits on starburst intensities, based on the maximum stellar mass remaining at high densities at $z = 0$, and find some tension between these and estimated number counts of sub-millimetre galaxies from Chapman et al. (2005). This implies that some change may be necessary in either the number counts themselves, the bolometric corrections used to convert these observations to total IR luminosities or the stellar IMF used to convert between the SFR and IR luminosity. However, the observations remain considerably uncertain, with the bolometric corrections relying sensitively on assumed dust temperatures, and the number counts subject to significant cosmic variance (see e.g. Austermann et al. 2009). More observations, at new wavelengths and in larger, independent fields, are needed to resolve these discrepancies.

We compare our constraints on these histories with recent predictions from galaxy formation models and simulations and find reasonably good agreement. Both exhibit similar tension with estimates of the high-redshift, extremely luminous number densities. However, the models are able to match the inferred number densities presented here *without* any change to the stellar IMF or requiring other exotic physics. The systematic uncertainties in the models, especially at high redshift, are large, however, so the empirical constraints presented here provide a powerful new means of constraining the models and their input parameters.

For example, if models are constrained via e.g. a halo-occupation approach or otherwise, so as to match the observed merger fractions of galaxies as a function of redshift, then these numbers become relatively large (>10 per cent) at redshifts $z \gtrsim 2$ (see e.g. Kartaltepe et al. 2007; Bluck et al. 2009; Lin et al. 2008; Bundy et al. 2009; Conselice, Yang & Bluck 2009; Jogee et al. 2009; Hopkins et al. 2009i; Bridge et al. in preparation). The most common assumption in many analytic and semi-analytic models is that, in such a major merger, the entire galaxy gas supply is channelled into the starburst. This, however, coupled with the high observed merger fractions (and implied merger rates), would lead to an overprediction of the burst contribution to the SFR density, relative to our constraints here. For example, the predictions of such a model are given in Hopkins et al. (2006b), and rise to ∼20–50 per cent of the SFR density at $z > 1$–2. Recently, however, Hopkins et al. (2009c) have pointed out that the processes that lead to angular momentum loss by the gas – driving bursts in the first place – rely on the stellar component of merging systems, and so become less efficient as gas fractions increase. Including these physics in the models (as the current generation to which we compare does) leads

[6] Note that it is important here to distinguish estimates of the SFR *induced* by mergers, i.e. that above what some control population would exhibit, from that simply in ongoing/identifiable mergers (since many criteria identify mergers for a time-scale of ∼Gyr, much longer than the burst time-scale). For example, a merger fraction of 10 per cent would imply at least 10 per cent of star formation in ongoing mergers, even if there were no starbursts and those systems were only forming stars at the same rate as they would in isolation.

to an asymptotic maximum contribution to the SFR density similar to that found here, while still giving a good match to observed merger fractions.

Despite the simple nature of the assumptions involved in our analysis, we show in high-resolution hydrodynamic simulations that they work well in allowing us to recover the star formation histories of bursts (even where the simulated system is much more complex). Especially in a statistical sense, our numerical experiments suggest that this approach is robust to a variety of detailed deviations from our idealized assumptions. Testing this (even in a few objects) via high-resolution reconstruction of stellar populations in bursts, directly from their observed spatially resolved SEDs, would provide a powerful test of this. In so far as we have compared with different simulations and models, the dominant uncertainty in our analysis is the nature – in particular the slope, relevant for the extrapolation to high gas surface densities – of the Kennicutt (1998) law. We have considered a range of slopes suggested by different observations. Although they yield similar behaviour at moderate and low SFRs, after $\sim 10^8$ yr from the beginning of a burst, the predicted behaviour at very early times in the bursts is quite different. A larger Kennicutt (1998) relation index implies higher peak SFRs and more sharply peaked starbursts, increasing the predicted number counts of the most luminous sources and making it relatively more easy for models to account for the most extreme star-forming systems. It therefore remains of considerable importance for observations to probe both gas density measurements and full SFR indicators in extreme systems, at low and high redshifts.

Finally, we note that our analysis is only possible because, as indicated by basic dynamics, simulations and observations of stellar populations, starburst components of spheroids were formed in dissipational (i.e. gas-rich, at their centres), rapid star-forming events. The dissipationless 'envelopes' surrounding the central, dense components in spheroids were not formed in such a manner (again indicated by both their structural and kinematic properties, simulations of their formation and stellar population observations). Rather, they represent the debris of stars from discs which were formed pre-merger and assembled (and violently relaxed) dissipationlessly. These stars were formed over extended periods of time, with new gas accretion on to the disc fuelling new or continuous star formation (e.g. Kereš & Hernquist 2009), as opposed to a single massive inflow. Especially in the most massive systems, they are also assembled from multiple systems via e.g. minor mergers contributing tidal material to the extended 'wings' well known in massive galaxies. As such, there is no straightforward means to invert their surface stellar mass density profiles to obtain their star formation history. Such constraints will depend on other methods, such as e.g. direct stellar population analysis. It should be borne in mind that this represents $\sim$90 per cent of the mass in most spheroids, and so understanding star formation in discs remains critical to understanding the origin of stellar populations in spheroids.

ACKNOWLEDGMENTS

We thank Chris Hayward and Josh Younger for helpful discussions throughout the development of this paper. Support for PFH was provided by the Miller Institute for Basic Research in Science, University of California Berkeley.

REFERENCES

Austermann J. E. et al., 2009, MNRAS, in press (arXiv:0907.1093) (doi:10.1111/j.1365-2966.2009.15620.x)
Avila-Reese V., Zavala J., Firmani C., Hernández-Toledo H. M., 2008, AJ, 136, 1340
Babbedge T. S. R. et al., 2006, MNRAS, 370, 1159
Balcells M., Graham A. W., Peletier R. F., 2007a, ApJ, 665, 1084
Balcells M., Graham A. W., Peletier R. F., 2007b, ApJ, 665, 1104
Barnes J. E., 1998, in, Kennicutt R. C.Jr.Schweizer F., Barnes J. E., Friedli D., Martinet L., Pfenniger D., eds, Saas-Fee Advanced Course 26: Galaxies: Interactions and Induced Star Formation. Springer-Verlag, Berlin, p. 275
Barnes J. E., Hernquist L. E., 1991, ApJ, 370, L65
Barnes J. E., Hernquist L., 1996, ApJ, 471, 115
Bell E. F., de Jong R. S., 2001, ApJ, 550, 212
Bell E. F., McIntosh D. H., Katz N., Weinberg M. D., 2003, ApJS, 149, 289
Bell E. F. et al., 2005, ApJ, 625, 23
Bender R., Doebereiner S., Moellenhoff C., 1988, A&AS, 74, 385
Bender R., Burstein D., Faber S. M., 1992, ApJ, 399, 462
Bender R., Burstein D., Faber S. M., 1993, ApJ, 411, 153
Bender R., Saglia R. P., Gerhard O. E., 1994, MNRAS, 269, 785
Bernardi M., Nichol R. C., Sheth R. K., Miller C. J., Brinkmann J., 2006, AJ, 131, 1288
Bernardi M., Shankar F., Hyde J. B., Mei S., Marulli F., Sheth R. K., 2009, MNRAS, in press (arXiv:0910.1093)
Bezanson R., van Dokkum P. G., Tal T., Marchesini D., Kriek M., Franx M., Coppi P., 2009, ApJ, 697, 1290
Bigiel F., Leroy A., Walter F., Brinks E., de Blok W. J. G., Madore B., Thornley M. D., 2008, AJ, 136, 2846
Binggeli B., Sandage A., Tammann G. A., 1985, AJ, 90, 1681
Bluck A. F. L., Conselice C. J., Bouwens R. J., Daddi E., Dickinson M., Papovich C., Yan H., 2009, MNRAS, 394, L51
Bothwell M. S., Kennicutt R. C., Lee J. C., 2009, MNRAS, 400, 154
Bouché N. et al., 2007, ApJ, 671, 303
Bridge C. R. et al., 2007, ApJ, 659, 931
Brinchmann J. et al., 1998, ApJ, 499, 112
Bruzual G., Charlot S., 2003, MNRAS, 344, 1000
Buat V., Burgarella D., 1998, A&A, 334, 772
Bundy K., Fukugita M., Ellis R. S., Targett T. A., Belli S., Kodama T., 2009, ApJ, 697, 1369
Bundy K. et al., 2006, ApJ, 651, 120
Bundy K. et al., 2008, ApJ, 681, 931
Bussmann R. S. et al., 2009, ApJ, 705, 184
Caldwell N., Rose J. A., Concannon K. D., 2003, AJ, 125, 2891
Caon N., Capaccioli M., Rampazzo R., 1990, A&AS, 86, 429
Caon N., Capaccioli M., D'Onofrio M., 1994, A&AS, 106, 199
Cappellari M. et al., 2007, MNRAS, 379, 418
Caputi K. I. et al., 2007, ApJ, 660, 97
Casey C. M. et al., 2009, MNRAS, 399, 121
Cattaneo A., Dekel A., Devriendt J., Guiderdoni B., Blaizot J., 2006, MNRAS, 370, 1651
Chabrier G., 2003, PASP, 115, 763
Chapman S. C., Blain A. W., Smail I., Ivison R. J., 2005, ApJ, 622, 772
Chapman S. C., Blain A., Ibata R., Ivison R. J., Smail I., Morrison G., 2009, ApJ, 691, 560
Cimatti A. et al., 2008, A&A, 482, 21
Ciotti L., Ostriker J. P., 2007, ApJ, 665, 1038
Ciotti L., Lanzoni B., Volonteri M., 2007, ApJ, 658, 65
Conselice C. J., Yang C., Bluck A. F. L., 2009, MNRAS, 394, 1956
Côté P. et al., 2006, ApJS, 165, 57
Côté P. et al., 2007, ApJ, 671, 1456
Courteau S., Dutton A. A., van den Bosch F. C., MacArthur L. A., Dekel A., McIntosh D. H., Dale D. A., 2007, ApJ, 671, 203
Covington M., Dekel A., Cox T. J., Jonsson P., Primack J. R., 2008, MNRAS, 384, 94
Cox T. J., Dutta S. N., Di Matteo T., Hernquist L., Hopkins P. F., Robertson B., Springel V., 2006, ApJ, 650, 791
Cox T. J., Jonsson P., Somerville R. S., Primack J. R., Dekel A., 2008, MNRAS, 384, 386
Croton D. J. et al., 2006, MNRAS, 365, 11
Dasyra K. M. et al., 2006, ApJ, 638, 745
Dasyra K. M. et al., 2007, ApJ, 657, 102

Dasyra K. M., Yan L., Helou G., Surace J., Sajina A., Colbert J., 2008, ApJ, 680, 232
Davis L. E., Cawson M., Davies R. L., Illingworth G., 1985, AJ, 90, 169
de Lucia G., Blaizot J., 2007, MNRAS, 375, 2
De Lucia G., Springel V., White S. D. M., Croton D., Kauffmann G., 2006, MNRAS, 366, 499
Dey A. et al., 2008, ApJ, 677, 943
di Matteo P., Combes F., Melchior A.-L., Semelin B., 2007, A&A, 468, 61
Doyon R., Wells M., Wright G. S., Joseph R. D., Nadeau D., James P. A., 1994, ApJ, 437, L23
Driver S. P., Allen P. D., Liske J., Graham A. W., 2007, ApJ, 657, L85
Emsellem E. et al., 2004, MNRAS, 352, 721
Emsellem E. et al., 2007, MNRAS, 379, 401
Faber S. M. et al., 1997, AJ, 114, 1771
Faucher-Giguère C.-A., Lidz A., Hernquist L., Zaldarriaga M., 2008, ApJ, 688, 85
Ferrarese L. et al., 2006, ApJS, 164, 334
Foster C., Proctor R. N., Forbes D. A., Spolaor M., Hopkins P. F., Brodie J. P., 2009, MNRAS, in press (doi:10.1111/j.1365-2966.2009.15606.x)
Gallagher J. S. III, Ostriker J. P., 1972, AJ, 77, 288
Gallazzi A., Charlot S., Brinchmann J., White S. D. M., Tremonti C. A., 2005, MNRAS, 362, 41
Gallazzi A., Charlot S., Brinchmann J., White S. D. M., 2006, MNRAS, 370, 1106
Genzel R., Tacconi L. J., Rigopoulou D., Lutz D., Tecza M., 2001, ApJ, 563, 527
Haiman Z., Jimenez R., Bernardi M., 2007, ApJ, 658, 721
Hernquist L., Spergel D. N., Heyl J. S., 1993, ApJ, 416, 415
Hibbard J. E., Yun M. S., 1999, ApJ, 522, L93
Hopkins A. M., Beacom J. F., 2006, ApJ, 651, 142
Hopkins P. F., Hernquist L., Cox T. J., Robertson B., Springel V., 2006a, ApJS, 163, 50
Hopkins P. F., Somerville R. S., Hernquist L., Cox T. J., Robertson B., Li Y., 2006b, ApJ, 652, 864
Hopkins P. F., Bundy K., Hernquist L., Ellis R. S., 2007, ApJ, 659, 976
Hopkins P. F., Cox T. J., Hernquist L., 2008a, ApJ, 689, 17
Hopkins P. F., Cox T. J., Kereš D., Hernquist L., 2008b, ApJS, 175, 390
Hopkins P. F., Hernquist L., Cox T. J., Dutta S. N., Rothberg B., 2008c, ApJ, 679, 156 (H08c)
Hopkins P. F., Hernquist L., Cox T. J., Kereš D., 2008d, ApJS, 175, 356
Hopkins P. F., Bundy K., Murray N., Quataert E., Lauer T. R., Ma C.-P., 2009a, MNRAS, 398, 898
Hopkins P. F., Cox T. J., Dutta S. N., Hernquist L., Kormendy J., Lauer T. R., 2009b, ApJS, 181, 135 (H09b)
Hopkins P. F., Cox T. J., Younger J. D., Hernquist L., 2009c, ApJ, 691, 1168
Hopkins P. F., Hernquist L., Cox T. J., Kereš D., Wuyts S., 2009d, ApJ, 691, 1424
Hopkins P. F., Lauer T. R., Cox T. J., Hernquist L., Kormendy J., 2009e, ApJS, 181, 486 (H09e)
Hopkins P. F., Murray N., Quataert E., Thompson T. A., 2009f, MNRAS, in press (arXiv:0908.4088)
Hopkins P. F. et al., 2009g, MNRAS, 397, 802
Hopkins P. F., Bundy K., Hernquist L., Wuyts S., Cox T. J., 2009h, MNRAS, in press (doi:10.1111/j.1365-2966.2009.15699.x)
Hopkins P. F. et al., 2009i, MNRAS, in press (arXiv:0906.5357)
Hopkins P. F., Younger J. D., Hayward C. C., Narayanan D., Hernquist L., 2009j, MNRAS, in press (arXiv:0911.1131)
Huang J.-S. et al., 2007, ApJ, 664, 840
James P., Bate C., Wells M., Wright G., Doyon R., 1999, MNRAS, 309, 585
Jesseit R., Naab T., Peletier R. F., Burkert A., 2007, MNRAS, 376, 997
Jesseit R., Cappellari M., Naab T., Emsellem E., Burkert A., 2009, MNRAS, 397, 1202
Jogee S. et al., 2009, ApJ, 697, 1971
Jonsson P., Cox T. J., Primack J. R., Somerville R. S., 2006, ApJ, 637, 255
Jonsson P., Groves B., Cox T. J., 2009, MNRAS, in press (arXiv:0906.2156)
Jørgensen I., Franx M., Hjorth J., van Dokkum P. G., 1999, MNRAS, 308, 833
Joseph R. D., Wright G. S., 1985, MNRAS, 214, 87
Kartaltepe J. S. et al., 2007, ApJS, 172, 320
Kennicutt R. C. Jr., 1998, ApJ, 498, 541
Kereš D., Hernquist L., 2009, ApJ, in press (arXiv:0905.2186)
Khochfar S., Burkert A., 2003, ApJ, 597, L117
Khochfar S., Silk J., 2006, ApJ, 648, L21
Kochanek C. S. et al., 2001, ApJ, 560, 566
Kormendy J., 1999, in Merritt D. R., Valluri M., Sellwood J. A., eds, ASP Conf. Ser. Vol. 182, Galaxy Dynamics – A Rutgers Symposium. Astron. Soc. Pac., San Francisco, p. 124
Kormendy J., Gebhardt K., Fisher D. B., Drory N., Macchetto F. D., Sparks W. B., 2005, AJ, 129, 2636
Kormendy J., Fisher D. B., Cornell M. E., Bender R., 2009, ApJS, 182, 216
Kuntschner H., Lucey J. R., Smith R. J., Hudson M. J., Davies R. L., 2001, MNRAS, 323, 615
Kuntschner H. et al., 2006, MNRAS, 369, 497
Laine S., van der Marel R. P., Lauer T. R., Postman M., O'Dea C. P., Owen F. N., 2003a, AJ, 125, 478
Laine S., van der Marel R. P., Rossa J., Hibbard J. E., Mihos J. C., Böker T., Zabludoff A. I., 2003b, AJ, 126, 2717
Lake G., Dressler A., 1986, ApJ, 310, 605
Lauer T. R., 1985, ApJS, 57, 473
Lauer T. R. et al., 1995, AJ, 110, 2622
Lauer T. R. et al., 2005, AJ, 129, 2138
Lauer T. R. et al., 2007, ApJ, 664, 226
Le Floc'h E. et al., 2005, ApJ, 632, 169
Li Y. et al., 2008, ApJ, 678, 41
Lin L. et al., 2008, ApJ, 681, 232
Liu Y., Zhou X., Ma J., Wu H., Yang Y., Li J., Chen J., 2005, AJ, 129, 2628
Lynden-Bell D., 1967, MNRAS, 136, 101
Magnelli B., Elbaz D., Chary R. R., Dickinson M., Le Borgne D., Frayer D. T., Willmer C. N. A., 2009, A&A, 496, 57
McDermid R. M. et al., 2006, MNRAS, 373, 906
McGaugh S. S., 2005, ApJ, 632, 859
Melbourne J. et al., 2008, AJ, 136, 1110
Menéndez-Delmestre K. et al., 2009, ApJ, 699, 667
Michard R., 2006, A&A, 449, 519
Mihos J. C., Hernquist L., 1994, ApJ, 431, L9
Mihos J. C., Hernquist L., 1996, ApJ, 464, 641
Naab T., Jesseit R., Burkert A., 2006, MNRAS, 372, 839
Naab T., Johansson P. H., Ostriker J. P., 2009, ApJ, 699, L178
Narayanan D., Cox T. J., Hayward C., Younger J. D., Hernquist L., 2009a, ApJ, in press (arXiv:0905.2184)
Narayanan D., Hayward C. C., Cox T. J., Hernquist L., Jonsson P., Younger J. D., Groves B., 2009b, ApJ, in press (arXiv:0904.0004)
Nelan J. E. et al., 2005, ApJ, 632, 137
Noeske K. G. et al., 2007a, ApJ, 660, L43
Noeske K. G. et al., 2007b, ApJ, 660, L47
Oñorbe J., Domínguez-Tenreiro R., Sáiz A., Artal H., Serna A., 2006, MNRAS, 373, 503
Papovich C., Dickinson M., Giavalisco M., Conselice C. J., Ferguson H. C., 2005, ApJ, 631, 101
Papovich C. et al., 2006, ApJ, 640, 92
Peletier R. F., Davies R. L., Illingworth G. D., Davis L. E., Cawson M., 1990, AJ, 100, 1091
Pérez-González P. G. et al., 2005, ApJ, 630, 82
Postman M., Lauer T. R., 1995, ApJ, 440, 28
Quillen A. C., Bower G. A., Stritzinger M., 2000, ApJS, 128, 85
Ravindranath S., Ho L. C., Peng C. Y., Filippenko A. V., Sargent W. L. W., 2001, AJ, 122, 653
Reda F. M., Proctor R. N., Forbes D. A., Hau G. K. T., Larsen S. S., 2007, MNRAS, 377, 1772
Reichardt C., Jimenez R., Heavens A. F., 2001, MNRAS, 327, 849
Rest A., van den Bosch F. C., Jaffe W., Tran H., Tsvetanov Z., Ford H. C., Davies J., Schafer J., 2001, AJ, 121, 2431
Robaina A. R. et al., 2009, ApJ, 704, 324
Robertson B., Cox T. J., Hernquist L., Franx M., Hopkins P. F., Martini P., Springel V., 2006, ApJ, 641, 21

Rothberg B., Joseph R. D., 2004, AJ, 128, 2098
Rothberg B., Joseph R. D., 2006a, AJ, 131, 185
Rothberg B., Joseph R. D., 2006b, AJ, 132, 976
Sajina A., Yan L., Armus L., Choi P., Fadda D., Helou G., Spoon H., 2007, ApJ, 664, 713
Sánchez-Blázquez P., Forbes D. A., Strader J., Brodie J., Proctor R., 2007, MNRAS, 377, 759
Sanders D. B., Mirabel I. F., 1996, ARA&A, 34, 749
Sanders D. B., Soifer B. T., Elias J. H., Madore B. F., Matthews K., Neugebauer G., Scoville N. Z., 1988, ApJ, 325, 74
Saunders W., Rowan-Robinson M., Lawrence A., Efstathiou G., Kaiser N., Ellis R. S., Frenk C. S., 1990, MNRAS, 242, 318
Schinnerer E. et al., 2008, ApJ, 689, L5
Schweizer F., 1996, AJ, 111, 109
Schweizer F., Seitzer P., 1998, AJ, 116, 2206
Schweizer F., Seitzer P., 2007, AJ, 133, 2132
Scoville N. Z., Sanders D. B., Sargent A. I., Soifer B. T., Scott S. L., Lo K. Y., 1986, ApJ, 311, L47
Shankar F., Bernardi M., Haiman Z., 2009, ApJ, 694, 867
Shen S., Mo H. J., White S. D. M., Blanton M. R., Kauffmann G., Voges W., Brinkmann J., Csabai I., 2003, MNRAS, 343, 978
Shier L. M., Fischer J., 1998, ApJ, 497, 163
Simien F., Prugniel P., 1997a, A&AS, 122, 521
Simien F., Prugniel P., 1997b, A&AS, 126, 15
Simien F., Prugniel P., 1997c, A&AS, 126, 519
Soifer B. T., Neugebauer G., 1991, AJ, 101, 354
Somerville R. S., Hopkins P. F., Cox T. J., Robertson B. E., Hernquist L., 2008, MNRAS, 391, 481
Tacconi L. J., Genzel R., Lutz D., Rigopoulou D., Baker A. J., Iserlohe C., Tecza M., 2002, ApJ, 580, 73
Tacconi L. J. et al., 2006, ApJ, 640, 228
Tacconi L. J. et al., 2008, ApJ, 680, 246
Thomas D., Maraston C., Bender R., Mendes de Oliveira C., 2005, ApJ, 621, 673
Titus T. N., Spillar E. J., Johnson P., 1997, AJ, 114, 958
Toomre A., 1977, in Tinsley B. M., Larson R. B., eds, Evolution of Galaxies and Stellar Populations. Yale University Observatory, New Haven, p. 401
Trager S. C., Faber S. M., Worthey G., González J. J., 2000, AJ, 119, 1645
Trager S. C., Somerville R. S., 2009, MNRAS, 395, 608
Trujillo I. et al., 2006, MNRAS, 373, L36
Valiante E., Lutz D., Sturm E., Genzel R., Chapin E., 2009, ApJ, 701, 1814
van Dokkum P. et al., 2008, ApJ, 677, L5
Veilleux S. et al., 2009, ApJS, 182, 628
Vika M., Driver S. P., Graham A. W., Liske J., 2009, MNRAS, in press (arXiv:0908.2102) (doi:10.1111/j.1365-2966.2009.15544.x)
Walter F., Riechers D., Cox P., Neri R., Carilli C., Bertoldi F., Weiss A., Maiolino R., 2009, Nat, 457, 699
Weinzirl T., Jogee S., Khochfar S., Burkert A., Kormendy J., 2009, ApJ, 696, 411
Wuyts S., Franx M., Cox T. J., Hernquist L., Hopkins P. F., Robertson B. E., van Dokkum P. G., 2009, ApJ, 696, 348
Yan L. et al., 2007, ApJ, 658, 778
Younger J. D. et al., 2007, ApJ, 671, 1531
Younger J. D. et al., 2008, ApJ, 688, 59
Younger J. D., Hayward C. C., Narayanan D., Cox T. J., Hernquist L., Jonsson P., 2009, MNRAS, 396, L66
Yun M. S., Reddy N. A., Condon J. J., 2001, ApJ, 554, 803

This paper has been typeset from a TEX/LATEX file prepared by the author.